Australian Meteorological and Oceanographic Journal 63 (2013) 41–64

The ACCESS coupled model: description, control climate and evaluation

Daohua Bi[1], Martin Dix[1], Simon J. Marsland[1], Siobhan O'Farrell[1], Harun A. Rashid[1], Petteri Uotila[1], Anthony C. Hirst[1], Eva Kowalczyk[1], Maciej Golebiewski[5], Arnold Sullivan[1], Hailin Yan[1], Nicholas Hannah[1], Charmaine Franklin[1], Zhian Sun[2], Peter Vohralik[3], Ian Watterson[1], Xiaobing Zhou[2], Russell Fiedler[4], Mark Collier[1], Yimin Ma[2], Julie Noonan[1], Lauren Stevens[1], Peter Uhe[1], Hongyan Zhu[2], Stephen M. Griffies[6],Richard Hill[7], Chris Harris[7], and Kamal Puri[2]

[1]CAWCR/CSIRO Marine and Atmospheric Research, Aspendale, Australia
[2]CAWCR/Bureau of Meteorology, Melbourne, Australia
[3]CSIRO Materials Science and Engineering, Lindfield, Australia
[4]CAWCR/CSIRO Marine and Atmospheric Research, Hobart, Australia
[5]CSIRO High Performance Computing and Communications Centre, Melbourne, Australia
[6]NOAA/Geophysical Fluid Dynamics Laboratory, Princeton, NJ, USA
[7]Met Office Hadley Centre, Exeter, UK

(Manuscript received July 2012; revised December 2012)

The Australian Community Climate and Earth System Simulator coupled model (ACCESS-CM) has been developed at the Centre for Australian Weather and Climate Research (CAWCR), a partnership between CSIRO[1] and the Bureau of Meteorology. It is built by coupling the UK Met Office atmospheric unified model (UM), and other sub-models as required, to the ACCESS ocean model, which consists of the NOAA/GFDL[2] ocean model MOM4p1 and the LANL[3] sea-ice model CICE4.1, under the CERFACS[4] OASIS3.2–5 coupling framework. The primary goal of the ACCESS-CM development is to provide the Australian climate community with a new generation fully coupled climate model for climate research, and to participate in phase five of the Coupled Model Inter-comparison Project (CMIP5). This paper describes the ACCESS-CM framework and components, and presents the control climates from two versions of the ACCESS-CM, ACCESS1.0 and ACCESS1.3, together with some fields from the 20th century historical experiments, as part of model evaluation. While sharing the same ocean sea-ice model (except different setups for a few parameters), ACCESS1.0 and ACCESS1.3 differ from each other in their atmospheric and land surface components: the former is configured with the UK Met Office HadGEM2 (r1.1) atmospheric physics and the Met Office Surface Exchange Scheme land surface model version 2, and the latter with atmospheric physics similar to the UK Met Office Global Atmosphere 1.0 including modifications performed at CAWCR and the CSIRO Community Atmosphere Biosphere Land Exchange land surface model version 1.8. The global average annual mean surface air temperature across the 500-year preindustrial control integrations show a warming drift of 0.35 °C in ACCESS1.0 and 0.04 °C in ACCESS1.3. The overall skills of ACCESS-CM in simulating a set of key climatic fields both globally and over Australia significantly surpass those from the preceding CSIRO Mk3.5 model delivered to the previous coupled model inter-comparison. However, ACCESS-CM, like other CMIP5 models, has deficiencies in various aspects, and these are also discussed.

[1]Commonwealth Scientific and Industrial Research Organisation.
[2]National Oceanic and Atmospheric Administration/Geophysical Fluid Dynamics Laboratory, Princeton, NJ, USA.
[3]Los Alamos National Laboratory, Los Alamos, NM, USA.
[4]Centre Européen de Recherche et de Formation Avancée en Calcul Scientifique, Toulouse, France.

Corresponding author address: Daohua Bi. Email: dave.bi@csiro.au

Introduction

There are many outstanding limitations on our scientific understanding of key aspects of the climate system response to anthropogenic climate forcing. For example, there are uncertainties concerning our understanding of the relative strength of the climate feedbacks and the climate sensitivity (e.g. Meehl et al. 2007), and of the response in the strength of the hydrological cycle (e.g. Durack et al. 2012).With regard to the Australian region, there is uncertainty concerning the response of key features of the climate state such as storm tracks (e.g. Trenberth and Fasullo 2010), and of the modes of variability affecting Australian climate (e.g. Cai et al. 2009, Zheng et al. 2010, Collins et al. 2010). All these uncertainties impact our ability to project climate change at the regional level and evaluate the potential impact on the Australian community, and to respond to the risks in an informed manner.

Puri et al. (2013) have outlined the development of a new Australian capacity in weather and climate simulation, the Australian Community Climate and Earth System Simulator (ACCESS). A major goal of ACCESS is to provide state-of-the-art climate modelling capacity to support Australian research aimed at addressing uncertainties such as those above. The priority initial aim in this area is to develop the coupled climate model for climate change simulation with the timeline driven by research community uptake relating to: (1) utilisation of the model results in analysis studies supporting the Fifth Assessment Report of the Intergovernmental Panel on Climate Change (IPCC AR5) and (2) utilisation of the model system by new Australian initiatives such as the Australian Research Council (ARC) Centre of Excellence for Climate System Science.

The set of papers in this special issue of the *Australian Meteorological and Oceanographic Journal* (AMOJ) describes the newly developed ACCESS climate model and evaluates its simulations, which are participating in the Coupled Model Intercomparison Project phase 5 (CMIP5) (Taylor et al. 2012). The CMIP5 model output data will form the basis of the model analyses to be used in the IPCC AR5. Participation in CMIP5 also facilitates the benchmarking of the ACCESS model against other models, and the ready dissemination of the output fields to users nationally and internationally via the earth system grid (ESG) (Williams et al. 2009). In this paper, the 'Model description' section describes all the components of the ACCESS coupled model, including the sub-models, coupler, coupling framework and coupling methodology. 'Experimental design' documents the experimental designs, including sub-model initialisations, atmospheric forcing setups for both the preindustrial control runs and the 20th century historical simulations, and spin-up processes. 'Model results' presents results from the 500-year pre-industrial control and the historical simulations, to document and evaluate key aspects of the model performance. The last section, 'Summary and conclusion', summarises the model skills and shortcomings and gives conclusions and perspectives. More detailed analyses of the model results from the ACCESS CMIP5 experiments in terms of performance of the individual sub-systems (i.e. atmosphere, land, sea-ice, and ocean), and investigations of some specific scientific issues and topics such as climate variability will be presented in papers (Dix et al. 2013, Kowalczyk et al. 2013, Uotila et al 2013, Marsland et al. 2013, Rashid et al. 2013a, Rashid et al. 2013b, Bi et al. 2013, Sun et al. 2013) that also appear in this issue.

Model description

This section describes the two versions of the ACCESS coupled model (hereafter 'ACCESS-CM') contributing to CMIP5, namely 'ACCESS1.0' and 'ACCESS1.3'. The components of ACCESS-CM are illustrated in Fig. 1. The atmospheric component is the UK Meteorological Office (hereafter 'Met Office') unified model (hereafter UM) (Davies et al. 2005; Martin et al. 2010, 2011). The ocean is the NOAA/GFDL MOM4p1 (Griffies 2009), and the sea-ice is the LANL CICE4.1 (Hunke and Lipscomb 2010) model. The atmosphere, together with the land surface model Met Office Surface Exchange Scheme version 2 (MOSES2, for ACCESS1.0) or CSIRO Community Atmosphere Biosphere Land Exchange version 1.8 (CABLE1.8, for ACCESS1.3), is coupled to ACCESS ocean model (ACCESS-OM; Bi et al. 2013), the ocean sea-ice core of ACCESS-CM, via the OASIS3.25 coupler (Valcke 2006).

The principal differences between the two versions of the ACCESS-CM are in their atmospheric and land surface components. ACCESS1.0, which may be considered our 'basic' version, includes the Met Office's well tested HadGEM2(r1.1) atmospheric physics and MOSES land surface model (Martin et al. 2011). ACCESS1.3 may be considered our 'aspirational' version. It includes significant new atmospheric physics similar to that of the Met Office Global Atmosphere (GA) 1.0 configuration (Hewitt et al. 2011)[5], and in particular the PC2 cloud scheme (Wilson et al. 2008). It also includes the Australian-developed CABLE1.8 land surface model (Kowalczyk et al. 2006, 2013). ACCESS1.3 is significantly more experimental than ACCESS1.0 as the new atmospheric physics has not been tested in century-scale climate change simulations previously[6]. As can be seen via comparison with Fig. 1 of Puri et al. (2013), the ACCESS1.3 configuration is a key step on the way to attaining a full earth system model as laid out in the original ACCESS project plan.

[5]GA1.0 comprises a suite of atmospheric model implementations sharing a common physics, and, of relevance here, includes the atmospheric component of the UK Met Office's HadGEM3(r1.1) coupled model (Arribas et al.2011, Hewitt et al. 2011)

[6]A version of the model with HadGEM2(r1.1) atmospheric physics and CABLE, denoted 'ACCESS1.1', experienced technical difficulties such that any results would have been too late for IPCC AR5 timelines. A version of the model the same as ACCESS1.3 but including a version of the MOSES land surface model was also developed, and denoted 'ACCESS1.2'. This version ultimately offered insufficient strategic or scientific advantage over ACCESS1.3, and has been discontinued.

Fig. 1. ACCESS-CM components and coupling framework. The system is built under framework of the Ocean, Atmosphere, Sea-ice, Soil (OASIS, version 3.25) coupler, which is developed at the Centre Européen de Recherche et de Formation Avancée en Calcul Scientifique (CERFACS), Toulouse, France.

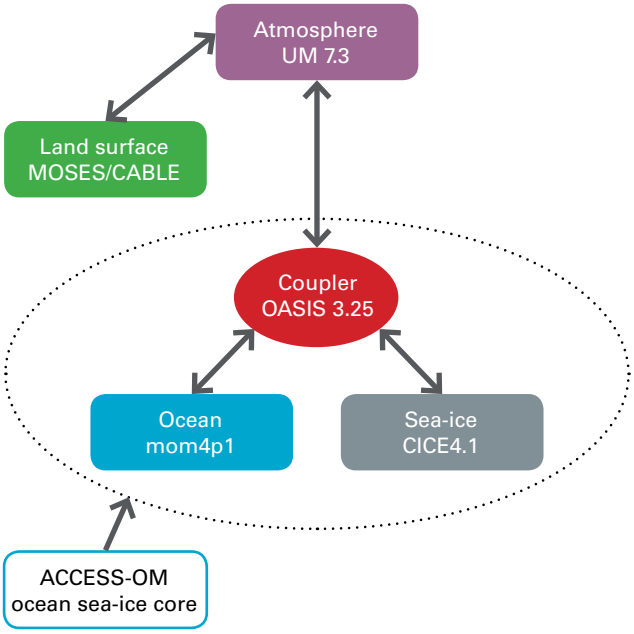

Though the component codes may be different, the ACCESS modelling program builds on a long history of weather and climate modelling in Australia. The history of Australian climate modelling is detailed in Smith (2007). The ultimate climate model of the preceding series, the CSIRO Mk3.6 (Rotstayn et al. 2012), is also featured extensively in this issue of AMOJ. Expertise from the earlier modelling has been beneficial in developing the weather and climate applications of ACCESS in a timely manner.

The remainder of this section provides more detail on each of the model components and on the coupling strategy. Readers are directed to the associated literature including user guides and manuals for full scientific and technical information about each component.

Atmospheric component

The ACCESS-CM uses the Met Office unified model (UM) as its atmospheric component. The atmospheric configuration in ACCESS1.0 is designed to be the same as that of HadGEM2 version r1.1 (Martin et al. 2011)[7], which is essentially the same as that in the HadGEM2 model versions used for CMIP5. The atmospheric configuration in ACCESS1.3 is as in ACCESS1.0 except in the physical parameterisation, which is similar to that of the Met Office's Global Atmosphere (GA) 1.0 (as in Arribas et al. 2011, and Hewitt et al. 2011) and includes modifications made at CAWCR.

[7]The base code used for the ACCESS1.0 atmospheric component is the UM code version 7.3 (UM7.3) external release, as this contains code required for coupling via OASIS. The default atmospheric physics in this code version is GA1.0, so the HadGEM2 (r1.1) physics codes needed to be re-introduced.

Resolution, dynamics and orography

The resolution is the same as is standard in the Met Office's HadGEM2 family of models (Martin et al. 2011) and also in early configurations of the HadGEM3 model (Arribas et al. 2011, Hewitt et al. 2011), namely a horizontal resolution of 1.25° latitude by 1.875° longitude (referred to as 'N96'), and 38 levels in the vertical.

The dynamics is as described in Davies et al. (2005) and is non-hydrostatic, fully compressible and uses a semi-Lagrangian advection scheme. The Arakawa 'C' grid (Arakawa and Lamb 1977) is used in the horizontal. The vertical coordinate is height-based and terrain-following.

The orography is derived from the 30″ GLOBE data set (GLOBE Task Team and others 1999), and the basic orography is the same for both ACCESS1.0 and ACCESS1.3. However, the GLOBE data set is found to have substantial deficiencies over Australia, and so instead the Geoscience Australia high-quality data set (Hilton et al. 2003) is used over Australia for all applications of ACCESS. This change makes some difference even at the N96 resolution (e.g. 50 m elevation change over the Great Dividing Range).

Physical parameterisations

ACCESS1.0

The atmospheric physical parameterisations in ACCESS1.0 are as in HadGEM2 version r1.1 (Martin et al. 2011, see also Martin et al. 2006; Collins et al. 2008; Martin et al. 2010). A brief summary follows.

The radiation scheme is that of Edwards and Slingo (1996). The radiative effects of the absorbing gases H_2O, CO_2, O_3, N_2O, CH_4, CFC11, CFC12 and O_2 are included. Parameterisations for 20 aerosol species are implemented in the scheme; these include major species such as sulphate, organic carbon, dust and sea salt. The radiation time step is set to give eight radiation calculations per day.

The turbulent fluxes of heat, moisture and horizontal momentum in the boundary layer are represented by the first order K profile closure as described by Lock et al. (2000). The scheme has a non-local mixing component for unstable boundary layers, and uses the 'SHARPEST' stability function (King et al. 2001; Edwards et al. 2006) for stable boundary layers.

The gravity wave drag scheme includes the orographic gravity wave component of Webster et al. (2003), which allows for blocking by sub-gridscale orography as well as gravity wave drag and has been shown to improve the general circulation (e.g. Webster et al 2003).

The convection scheme is a modified mass flux scheme based on Gregory and Rowntree (1990). Initiation of convection is based on evaluation of undiluted parcel ascent from the near surface, which is used to determine whether convection is possible from the boundary layer. Categorisation of convection as deep or shallow depends on the level of the cloud top. Representations of convective momentum transport (CMT) are included for both deep and shallow convection.

The precipitation microphysics is determined by the Wilson and Ballard (1999) single moment bulk scheme, which features explicit calculations of transfer between vapour, liquid and ice phases. The prognostic ice variable is split by a diagnostic relationship into ice crystals and aggregates, which are treated separately in the microphysical transfer terms before being recombined after the calculations. The condensation and evaporation of cloud water is calculated within the diagnostic cloud scheme.

ACCESS1.0 uses the Smith (1990) diagnostic cloud scheme that is based on a sub-grid probability distribution of a temperature and a moisture variable, with the liquid cloud amount then being derived using a critical relative humidity. The scheme has been modified such that the prognostic ice variable is used to diagnostically calculate the ice cloud fraction (Wilson et al. 2004).

The physical parameterisations in ACCESS1.0 are mostly common to the ACCESS NWP model described in Puri et al. (2013). There are two exceptions involving: (1) the specification in the stability function in the stable boundary layer, and (2) the usage of an additional, non-orographic, gravity wave drag term in the NWP model (Warner et al. 2005), where more detailed discussion of the above physical parameterisations may be found.

ACCESS1.3

The atmospheric physical parameterisations in ACCESS1.3 are similar to GA1.0 (Arribas et al. 2011, Hewitt et al. 2011). Parameterisation differences between ACCESS1.0 and ACCESS1.3 are described below.

The radiation scheme in ACCESS1.3 is modified to include the 'Tripleclouds' scheme developed by Shonk and Hogan (2008) to represent horizontal cloud inhomogeneity. A detailed description of this scheme and its evaluation within the ACCESS model are provided by Sun et al. (2013). This implementation differs from the simpler scaling scheme implemented in GA1.0 to account for cloud inhomogeneity (Hewitt et al. 2011). Both approaches increase radiative transmissivity in cloudy grid boxes. The radiation scheme in ACCESS1.3 follows GA1.0 in including improved pressure and temperature scaling (Hewitt et al. 2011). This change mainly improves simulation of long-wave fluxes in the middle atmosphere.

The boundary layer physics in ACCESS1.3 is mostly as in ACCESS1.0. However, algorithms for momentum, sensible and latent heat flux at the air-sea interface have been modified from those in both ACCESS1.0 and in GA1.0 based on results from field programs (Fairall et al. 2003). The modifications involve the empirical expressions for momentum and scalar atmospheric surface roughness lengths for 10 m neutral wind speeds. The modified algorithms are found to ease certain biases in the pattern of global sea surface temperature (SST) distribution, including a mild reduction in the equatorial Pacific cold tongue bias.

ACCESS1.3 follows GA1.0 in using a 'buddy' scheme for coastal grid points to split the near-surface winds into separate components over the ocean and the land portions (Hewitt et al. 2011). This scheme was found in GA1.0 to significantly increase (i.e. improve) precipitation over the maritime continent. ACCESS1.3 does not follow GA1.0 in using the boundary layer solver of Wood et al. (2007) due to technical issues associated with the use of the CABLE land surface model, and instead retains the ACCESS1.0 formulation.

The convection physics in ACCESS1.3 is mostly similar to that in ACCESS1.0. ACCESS1.3 follows GA1.0 in using revised parcel perturbations for shallow convection that help make vertical fluxes more consistent between the boundary layer and convection schemes (Hewitt et al. 2011). ACCESS1.3 retains the CAPE closure scheme based on relative humidity of ACCESS1.0, instead of the GA1.0 closure scheme based on vertical wind speed.[8,9]

ACCESS1.3 uses the prognostic cloud prognostic condensate (PC2) scheme (Wilson et al. 2008), as does GA1.0. PC2 includes prognostic variables for cloud liquid water content, ice water content, liquid cloud fraction, ice cloud fraction and total cloud fraction. Each process in the model acts as a source/sink of these prognostic variables, including the convection scheme, so that PC2 represents both convective and large-scale cloud in the model. The GA1.0 implementation of the PC2 scheme is modified through use of the parameterisation of Franklin et al. (2012) to modify the PC2 ice cloud fraction and the cloud area scheme of Boutle and Morcrette (2010) to account for the effects of coarse vertical resolution on low-level cloud cover.

Aerosol parameterisation

The aerosol scheme used for both ACCESS1.0 and 1.3 is the Coupled Large-scale Aerosol Simulator for Studies in Climate (CLASSIC) (Bellouin et al. 2011). The scheme is used to simulate seven aerosol species, some with multiple components: mineral dust, sea salt, fossil fuel black carbon (FFBC), fossil fuel organic carbon (FFOC), biomass burning aerosols (with assumptions about the proportions of organic carbon and black carbon), secondary organic aerosols (from forest turpene), and sulphate aerosols (from dimethylsulphide (DMS) and SO_2 emissions and the sulphur cycle). All aerosol species exert a direct radiative effect. All species except mineral dust and FFBC aerosols (which are considered hydrophobic) exert first and second indirect effects. These are also referred to as the cloud albedo and

[8]The base code used for the ACCESS1.3 atmospheric component was a pre-release version of the UM7.3. This version included most of the GA1.0 physics, but did not include the change to vertical wind speed-based CAPE closure, and this was not upgraded separately for ACCESS1.3. The base physics for this pre-release version, on which CAWCR built, is as for the version denoted in the UM User Interface [UMUI] under job name ahhbs.

[9]A code error was inadvertently introduced during testing whereby the convective momentum transport (CMT) for deep convection in ACCESS1.3 was effectively turned off. Thus the current version of ACCESS1.3 does have CMT for shallow convection but not for deep convection. Deep convection CMT is known to have beneficial effects on the tropical solution (e.g. Wu et al. 2007, Kim et al. 2008), and will be rectified in a subsequent version.

cloud lifetime effects. All aerosol species are prognostic except for sea salt, which is diagnosed each time step based on the near-surface wind speed, and secondary organic aerosols (SAO), which are prescribed by a monthly varying climatology. Dust concentrations in ACCESS1.3 are essentially zero, due to further work being required on the CABLE/dust module interface. Aerosol treatments are the same in ACCESS1.0 and 1.3 in all other respects, and are described in more detail in Dix et al. (2013).

Land surface process

Climate models and numerical weather prediction require a description of the land surface and surface exchange processes. Land surface models (LSM) provide this information by calculating the turbulent transport of momentum, heat and water between the land surface, canopy and atmosphere. The thermal and hydrological processes in the soil and snow are also simulated. The complexity and accuracy of land surface models has increased over the last decade. They include improved representations of canopy processes, especially plant physiology to allow for fully interactive terrestrial carbon cycles.

To explore the range of interactions between vegetation behaviour and the atmosphere we are using two land surface models coupled to the atmospheric model in ACCESS (Kowalczyk et al. 2013). The ACCESS1.0 simulations use the same setup of the Met Office's Surface Exchange Scheme (MOSES) version 2.2 (Cox et al. 1999, Essery et al. 2003) as in HadGEM2(r1.1) (Martin et al. 2011). MOSES includes mechanistic formulations of the physical, biophysical and biogeochemical processes that control the exchange of momentum, radiation, heat, water and carbon fluxes between the land surface and the atmosphere. The land surface heterogeneity is described by having multiple surface types in each grid cell. For MOSES there are nine possible tiles for each grid cell and a separate energy balance is calculated for each tile. Area-weighted grid mean fluxes and temperatures are then calculated from the individual tile energy balances. The surface temperatures are computed from the same surface energy balance equation for each vegetated and non-vegetated tile. A homogeneous soil moisture and temperature exists for each tile within the grid.

For ACCESS1.3 the Community Atmosphere Biosphere Land Exchange (CABLE version 1.8) has been coupled to the UM. CABLE consists of a comprehensive description of the surface processes that calculate momentum, heat, water and carbon fluxes (Kowalczyk et al. 2006, Wang et al. 2010). CABLE has 13 surface tile types (ten vegetated tile and three non-vegetated tile types). The underlying soil is also tiled, allowing for sub-surface soil temperature and moisture tiling. CABLE was formulated on the basis of a multi-layer model (Leuning 1995) and represents the canopy as a one layer, two-leaf canopy as described in Wang and Leuning (1998). CABLE has been extensively evaluated (e.g. Wang et al. 2011), and a similar version has been coupled with a low resolution global circulation model and run for multi-hundred years to explore the impact of land use induced land cover change on climate extremes (Avila et al. 2012).

There are a number of differences in the representation of the canopy between CABLE and MOSES. Firstly, MOSES places the canopy alongside a bare ground tile (a horizontal tile approach), whereas CABLE conceptually places a canopy above the ground allowing for aerodynamic and radiative interaction between the canopy and the ground. Secondly, CABLE differentiates between sunlit and shaded leaves (two-leaf model) for the calculation of photosynthesis, stomatal conductance and leaf temperature. Finally CABLE includes a plant turbulence model to calculate the air temperature and humidity within the canopy.

MOSES uses prescribed surface albedo, including the soil albedo and canopy albedo. CABLE uses the same prescribed, spatially varying soil albedo but resolves the canopy albedo diurnally as a function of beam fraction, the sun angle, canopy leaf area index, leaf angle distribution and the transmittance and reflectance of the leaves. This results in generally smaller surface albedo than that used in MOSES (Kowalczyk et al. 2013).

Note that while MOSES and CABLE are both able to calculate carbon fluxes, these have not been assessed or submitted for the ACCESS1.0 and ACCESS1.3 simulations.

We define the UM-MOSES/CABLE grid land-sea mask, especially its fractional land-points at coastlines, by using the underlying ACCESS-OM land-sea mask to obtain the best consistency of land-sea mask between the atmosphere-land and ice-ocean subsystems. This is critical for ensuring conservation of river runoff when passed from the UM into CICE by the OASIS3 remapping. The resultant land fraction is used to scale up river runoff water volume before it is sent to the coupler. This is done to compensate for what would be remapped by OASIS3 onto land-points of the target grid and therefore lost in the masking. Doing so guarantees that the volume of water actually going into the ice-ocean system matches the real runoff amount diagnosed in the atmosphere-land component.

Ocean

The ocean component of ACCESS-CM is an implementation of the NOAA/GFDL MOM4p1 numerical code (Griffies 2009) which has previously been used as the ocean component for NOAA/GFDL contributions to CMIP3 (Griffies et al. 2005, Gnanadesikan et al. 2006) and CMIP5 (Griffies et al. 2011, Dunne et al. 2012). The ACCESS-CM implementation uses a Boussinesq (volume conserving) approximation for the ocean interior and real (mass) fluxes of freshwater at the upper surface for exchanges of precipitation, evaporation, runoff from land, and both the melting and freezing of sea-ice. This formulation permits a time varying ocean volume (and sea surface height) according to the conservation (or otherwise) of the hydrological cycling both within and between the various components of the ACCESS-CM. More details on the non-conservation of ocean mass in ACCESS1.0 and ACCESS1.3 are given in Marsland et al. (2013).

The ACCESS ocean model has 360 longitude by 300 latitude points on a logically rectangular matrix with 50 vertical levels. The horizontal discretisation is on an orthogonal curvilinear grid nominally one degree for both longitude and latitude. It has the following refinements: (1) a tripolar grid (Murray 1996) is used north of 65°N to preclude a singularity at the geographical north pole; (2) a cosine dependent (Mercator) grid is used south of 30°S to avoid large grid cell aspect ratios and also to better resolve zonal currents in the Southern Ocean and at the Antarctic margin; and, (3) a refinement of latitudinal spacing to 1/3° is applied between 10°S and 10°N to better resolve predominantly zonal equatorial ocean currents. The vertical discretisation employs the z^* coordinate of Adcroft and Campin (2004), and allows for partial grid cells at the base of the water column. The z^* formulation allows for the pressure loading of sea-ice to be accounted for when determining sea level evolution, and avoids the possibility of a disappearing upper ocean level in the case where sea-ice thickness exceeds the ocean's upper level thickness (10 m), while the atmospheric pressure is treated as a constant and thus ignored. There are 50 vertical levels spanning the 0–6000 m depth range, with 20 levels each of nominal 10 m thickness in the upper ocean. Below 200 m the vertical resolution smoothly decreases, with the deepest level having a thickness of approximately 333 m.

The prognostic variables are conservative temperature (McDougall 2003), salinity, 'zonal' and 'meridional' velocities locally aligned to the horizontal discretisation, and sea level displacement from an idealised sphere representing the ocean at rest. Details of the choices of ocean physics and sub-gridscale parameterisation settings used in the ACCESS1.0 and ACCESS1.3 simulations are documented in an accompanying ACCESS Ocean Model (ACCESS-OM) benchmarking paper (Bi et al. 2013), which compares ACCESS-OM performance in a Coordinated Ocean-ice Reference Experiment against simulations from other climate modelling centres (Griffies et al. 2009). The ocean component uses the K-profile parameterisation (KPP) scheme (Large et al. 1994); a modified skew diffusive flux form (Griffies 1998) of the Gent and McWilliams neutral sub-gridscale eddy advection parameterisation (Gent et al. 1995); and mixed layer restratification by submesoscale eddies following the scheme of Fox-Kemper et al. (2008, 2011).

There are two notable differences between the ACCESS-OM configurations used in Bi et al. (2013) and the ACCESS1.0 and ACCESS1.3 experiments as submitted to CMIP5. Firstly, the ACCESS-OM used an explicit convection scheme following Rahmstorf (1993), but the ACCESS1.0 and ACCESS1.3 models use an implicit convection scheme where instabilities are only partially removed via a large vertical diffusivity (0.1 $m^2\ s^{-1}$) which introduces a timescale for convective events rather than the instantaneous convection of the explicit scheme. Secondly, we note that both ACCESS-OM and the experiments considered here use a reduced background vertical diffusivity near the equator, with this diffusivity reducing to a minimum at the equator. This implementation is based both on the motivations and the scheme of Jochum (2009). Details of the implementation in ACCESS are given in Bi et al. (2013). However, outside of the equatorial band the ACCESS-OM experiment used a background vertical diffusivity of $1.0 \times 10^{-5}\ m^2\ s^{-1}$ while the ACCESS1.0 and ACCESS1.3 simulations used half that value ($0.5 \times 10^{-5}\ m^2\ s^{-1}$).

There are also two differences in the formulation of the ocean model between the ACCESS1.0 and ACCESS1.3 contributions to CMIP5. Firstly, as discussed by Rashid et al. (2013b) a key aspect of coupled model simulations is the representation of ENSO. The critical Richardson number in the KPP mixed layer scheme (Large et al. 1994) was halved from 0.3 in ACCESS1.3 to 0.15 in ACCESS1.0. This change was motivated by improved (increased) amplitude for peaks in the power spectrum of the Nino3 SST index of interannual variability in ACCESS1.0. Secondly, the time steps (3600 s) of the ocean model, the sea-ice model, and the coupling frequency between ocean and sea-ice models, were concurrently halved from 3600 to 1800 seconds as necessary to overcome infrequent and intermittent numerical instabilities in the ACCESS1.3 simulations. Further details of the ACCESS-OM component can be found in Bi et al. (2013), while a selection of supplementary ocean results from the ACCESS1.0 and ACCESS1.3 contributions to CMIP5 can be found in Marsland et al. (2013).

Sea-ice

The LANL CICE4.1 model represents the state-of-the-art in sea-ice modelling (e.g. Flocco et al. 2012, Holland et al. 2012) and has been designed to couple with the ocean and atmosphere components of climate models. CICE4.1 uses an elastic-viscous-plastic dynamics scheme (Hunke and Dukowicz 1997) for the internal ice stress, an incremental linear remapping for the ice advection term, and computes the ice thickness redistribution through ridging and rafting schemes by assuming an exponential redistribution function. The model is divided into five thickness categories of ice and open water. CICE in the ACCESS coupled system runs on the ocean grid which gives enhanced resolution in the Arctic due to the orthogonal curvilinear tripolar grid and in the Antarctic due to the Mercator grid with meridians converging at the South Pole (Bi and Marsland 2010, Uotila et al. 2012).

For coupling CICE to the atmospheric model (UM), a special thermodynamic configuration is enforced because of the implicit boundary layer scheme used in the UM over sea-ice. The UM atmospheric boundary layer scheme involves the direct calculation of sea-ice or snow surface temperature, and therefore for compatibility, CICE is not allowed to use its layered thermodynamics scheme and compute surface temperatures. Therefore, as in the Met Office HadGEM3(r1.1) model (Hewitt et al. 2011), CICE in the ACCESS model uses a so called zero-layer thermodynamic model (Semtner 1976), which is a simplified form of the layered sea-ice thermodynamic model with no heat storage

at all, except the latent heat associated with ice formation.

In addition, because of coupling to the UM, CICE employs a simplified sea-ice albedo parameterisation, where fixed albedo values are set in the UM radiation code for dry snow, wet melting snow and bare ice, with a reduction dependent on temperature near the melt point to simulate melt ponds. Whilst ACCESS1.0 uses the 'default' settings of albedos from the Met Office HADGEM2 (r1.1) model, ACCESS1.3 uses slightly larger values based on observations of Pirazzini (2008). This is for the purpose of enhancing the simulated ice thickness in the central Arctic and in the Southern Ocean, which was found to be excessively thin in ACCESS1.0. However this causes excessively thick ice next to the Antarctic continent that does not melt out each summer (see Fig. 12). Values of the thermodynamic and dynamic parameters used in the ACCESS-CM CMIP5 experiments are listed in Table 1.

Coupler and coupling strategy

The ACCESS-CM model uses the CERFACS OASIS3.2-5 coupler (hereafter OASIS3) (Valcke 2006). The implementation in the ACCESS-CM follows closely that in the ACCESS-OM described in Bi and Marsland (2010) and Bi et al. (2013). At run time, OASIS3 in the coupled model remains as a separate mono-process executable, receiving, interpolating, and sending coupling fields between the sub-models which also run as separate executables at the same time. As the ACCESS-CM configures CICE4.1 and MOM4p1 on the same global tripolar grid in the horizontal, and as both these components use the Arakawa B-grid, coupling between CICE4.1 and MOM4p1 is relatively straightforward.

In ACCESS-CM, as in the ACCESS-OM, the sea-ice model is literally placed between the atmospheric model and ocean model, working as a 'coupling medium' and technically being the only one that needs to communicate with the other two sub-models at the same time. Namely, all coupling fields from the source model (UM/MOM4p1) are gathered, processed jointly with the associated coupling fields from sea-ice itself where present, and then delivered to the target model (MOM4p1/UM). The above design has several technical advantages, including easy control over the coupling frequencies. The ACCESS-CM uses different frequencies for coupling atmosphere to sea-ice (every three hours, i.e. six atmospheric time steps) and sea-ice to ocean (every time step of the ice and ocean models, typically one hour). This coupling strategy is illustrated by Fig. 2 of Bi et al. (2013).

Use of OASIS3 requires the development of a coupling interface for each sub-model. The interface for the UM in both versions of the ACCESS-CM is based on that present in the UM7.3 code and used in HadGEM3 (r1.1) (Hewitt et al. 2011). In ACCESS-CM, this interface is slightly modified for connecting atmosphere to sea-ice and handling 42 two-dimensional coupling fields (24 from atmosphere to ice and 18 from ice to atmosphere) via OASIS3. Similarly, an interface is implemented in MOM4p1 for connecting ocean to sea-ice and handling 20 coupling fields (seven from ocean to ice and 13 from ice to ocean). In the 'coupling medium' CICE4.1, the interface is designed to connect ice to both atmosphere and ocean, handling (receiving, processing, and delivering) all the 62 coupling fields.

While the exchange of coupling data between ocean and sea-ice needs no transformation via the OASIS3 main process because of grid compatibility, the coupling fields between atmosphere and sea-ice are remapped by OASIS3 to the target grid using a first order conservative remapping algorithm of the Spherical Coordinate Remapping and Interpolation Package (SCRIP) (Jones 1997).

Experimental design

The experimental framework for the CMIP5 simulations for both ACCESS1.0 and ACCESS1.3 involves initialisation using near-present day conditions, a multi-century spin-up run using the CMIP5 preindustrial conditions, followed by commencement of the actual CMIP5 preindustrial control (hereafter piControl) and historical simulations at the same point. The spin-up runs for both versions were initialised using an atmospheric and land surface state obtained for 1 January 1979 from an atmospheric/land surface model simulation started using fields obtained from the Met Office for 30 September 1978, and ocean climatological temperature and salinity fields for January from the World Ocean Atlas 2005 (WOA2005; Locarnini et al. 2006, Antonov et al. 2006). The sea-ice model is initialised using the WOA2005 January sea surface temperature (SST) and salinity (SSS). Any grid point that has SST no higher than the SSS-dependent freezing point is set to have five thickness category ice areas which jointly fully cover the cell. While the 3 m thick category ice has the largest area within the cell, the average ice thickness for the cell is less than 3 m due to the nonlinear distribution of ice thickness.

Details of the forcing data for the CMIP5 simulations are given in Dix et al. (2013). For the preindustrial spin-up and CMIP5 piControl simulations, standard CMIP5 preindustrial (circa 1850) prescriptions are used for atmospheric concentrations of CO_2, CH_4, N_2O and O_3, the solar constant, and aerosol emissions. All these factors, together with atmospheric halocarbon concentrations and volcanic stratospheric aerosol load are set to vary according to the standard CMIP5 prescription in the historical simulation. The option to treat the preindustrial stratosphere as clear of volcanic aerosols (Taylor et al. 2009) is taken. (Note, however, that this will result overall in a slight cold bias in the historical simulation relative to the piControl, see Dix et al. (2013).) Finally, the seasonally-varying biogenic aerosol concentration and a background volcanic SO_2 out-gassing flux (into the lower to mid troposphere) are maintained throughout all simulations.

The preindustrial spin-up simulations for ACCESS1.0 and ACCESS1.3 are continued for 300 years and 250 years, respectively. Ideally, the spin-up simulation should continue until equilibrium is achieved prior to commencement of the

Table 1. Values of selected important dynamic and thermodynamic sea-ice model parameters used in the ACCESS CMIP5 experiments.

Short name	*Value*	*Full name*
cosw, sinw	16°	Ocean-ice turning angle
mu_rdg	3 $m^{1/2}$	Ridging parameter value
ALPHAC	0.78	Cold deep snow albedo in ACCESS 1.0
ALPHAC	0.84	Cold deep snow albedo in ACCESS 1.3
ALPHAB	0.61	Bare ice albedo in ACCESS 1.0
ALPHAB	0.68	Bare ice albedo in ACCESS 1.3
ALPHAM	0.65	Melting deep snow albedo in ACCESS1.0
ALPHAM	0.72	Melting deep snow albedo in ACCESS1.3
DTICE	0.5	Temperature range to determine snow melting in albedo calculation
DT_BARE	0.25	Temperature range to determine bare ice melting in albedo calculation
DALB_BARE_WET	–0.075	Albedo change to determine bare ice melting in albedo calculation
Dragio	0.00536	Ice-ocean drag
ustar_min	0.0005 m/s	Minimum ice-ocean friction velocity
Conduct	Bubbly	Ice conductivity option
Iceruf	0.0005 m	Surface roughness of ice
Chio	0.004	Ice-ocean heat exchange coefficient

historical simulation. However, the deep ocean is known to require thousands of years to reach equilibrium (e.g. Stouffer 2004) which is not possible given current resource constraints. Therefore, like other CMIP5 models (e.g. Griffies et al. 2011, Voldoire et al. 2012), the spin-up simulations for the ACCESS-CM are performed for an affordable length that yield adequate quasi-equilibria of the surface fields before the start of the CMIP5 historical and piControl simulations proper.

It should be noted that in the ACCESS1.3 spin-up phase, sea-ice albedos used for the first 149 years are also the 'default' setting for UM, i.e. the same as that used in ACCESS1.0. It was found that CABLE results in warmer surface air temperature which allows larger sea-ice albedos (closer to the Pirazzini 2008 observations) to be used for better model climate in terms of both ice and surface air temperature (SAT) distributions. Therefore, from year 150 of the spin-up onwards, ACCESS1.3 uses larger sea-ice albedos (Table 1). The effect of the albedo change on the surface energy budget contributes to the differences in residual drifts seen in the ACCESS1.0 and ACCESS1.3 solutions (see section 'Model results').

The 500 years of the CMIP5 piControl simulation for ACCESS1.0 covers years 300 through 799, and ACCESS1.3 years 250 through 749, from time of original initialisation. The historical simulations also commence at the beginning of year 300 and year 250 for ACCESS1.0 and 1.3, respectively. Hereafter, we will redesignate the first year of the CMIP5 piControl simulation in each case as '1850', for ease of comparison to the respective historical simulation. In the following, we will examine the extent of the residual model adjustments during the course of the piControl simulations. We will see that ACCESS1.0 displays a slight residual drift in surface properties, more than for ACCESS1.3, and this was the motivation for continuing the ACCESS1.0 pre-industrial spin-up for the slightly longer period. We will then provide an initial evaluation of certain aspects of the historical simulations during the instrumental period. Subsequent manuscripts in this issue of AMOJ will provide much more detailed documentation and evaluation of the model behaviour.

Model results

In this section we evaluate ACCESS-CM by presenting a selection of key fields from the piControl and historical simulations performed with the two versions, and comparing them against observations or their reanalysis estimations where appropriate. We define the 'control climatology' as the time average over the last 100 years of the 500-year piControl integrations and the 'present climate' as the 30-year average over 1976–2005 from the historical simulations.

Atmosphere

Control run global mean thermal equilibrium and drift at the surface

It is desirable that a coupled model used for climate change simulation and climate sensitivity research be able to hold a stable, realistic control climate, especially a thermal equilibrium at the surface. Fig. 2(a) shows the time series of the globally averaged annual mean SAT for the 500-year period of the ACCESS1.0 and ACCESS1.3 piControl runs. In the ACCESS1.0 case, we see a persistent increase of SAT in the course of the integration, and the final warming reaches about 0.35 °C, with the drift rate being 0.07 °C/century. This drift rate is modest in comparison to that found in the majority of CMIP3 models, where the median drift is approximately

Fig. 2. Evolution of the piControl annual mean global average: (a) SAT (°C) and (b) TOA energy budget (W m^{-2}). Thick lines are the linear regressions.

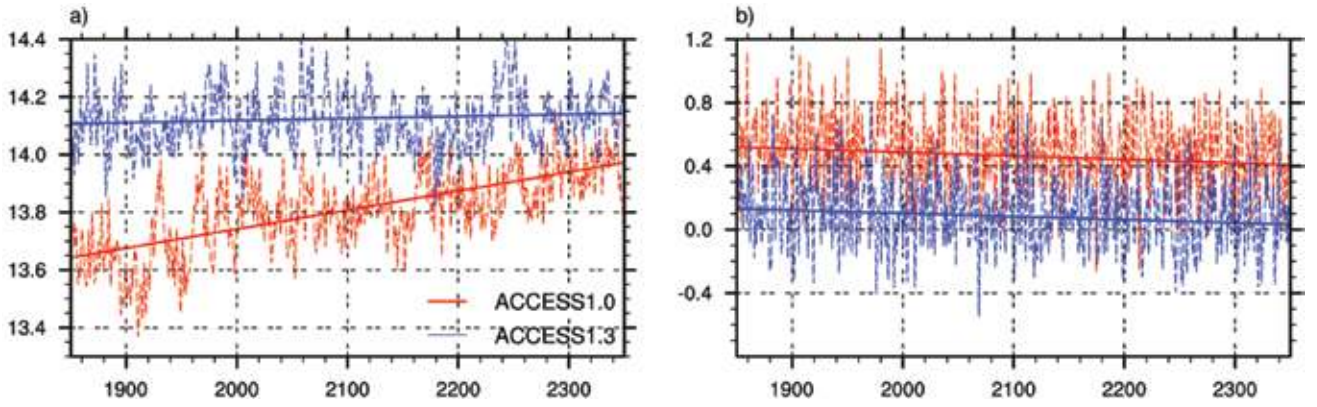

Fig. 3. Historical run present-day SAT biases (relative to ERA-Interim reanalysis 1979–2008 data): (a) ACCESS1.0 and (b) ACCESS1.3. Units are °C.

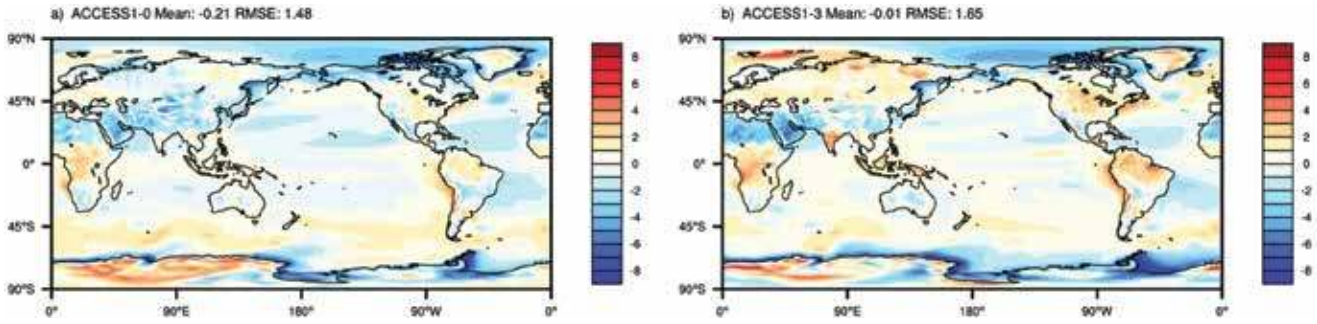

0.12 °C/century (Sen Gupta et al. 2012). For ACCESS1.3, the whole 500-year integration shows a minimal increase of SAT. The final warming is less than 0.04 °C and the trend is 0.008 °C/century.

Such a difference between the two versions indicates that ACCESS1.0 has a bigger deficiency in energy balance at the top of the atmosphere (TOA). This is confirmed by the time series of energy budget at the TOA shown in Fig. 2(b) where we see a considerable imbalance of heat fluxes throughout the ACCESS1.0 control run. It starts from a net energy gain of above 0.5 W m^{-2} and ends with a smaller value of around 0.4 W m^{-2} which is still quite far from the desirable ±0.1 W m^{-2} criteria for long control runs (e.g. Gent et al. 2011). In contrast the ACCESS1.3 shows a much smaller imbalance at the TOA through the 500-year control period. It starts from just above 0.1 W m^{-2} and ends with a very small positive imbalance of about 0.03 W m^{-2}.

Surface air temperature

Figure 3 presents the bias maps of the modelled near surface air temperature against the ERA-Interim reanalysis data (Dee et al. 2011) for the period of 1979–2008. Table 2 gives some details of the area averaged biases and root mean square errors (RMSEs) over land and oceans, in selected zonal bands for both ACCESS1.0 and ACCESS1.3, including the difference between the two models. The two model versions show generally very similar bias patterns. Particularly they both bear large cold biases over the polar regions, especially on the sea-ice adjacent to the Antarctic continent, the coasts of Greenland and the Canadian archipelagos. The ACCESS1.0 historical run simulates a lower present-day global mean SAT than ACCESS1.3 because it starts from a considerably cooler initial condition and never catches up with ACCESS1.3 during the course of the 156-year simulation, similar to that shown in Fig. 2(a) for the piControl runs. This difference in part reflects the different effects of the land surface models (i.e. MOSES and CABLE) in determining the model surface thermal states. Table 2 reveals that, except for Antarctica, all land is simulated significantly colder in ACCESS1.0 than in ACCESS1.3. ACCESS1.0 has a cold bias as large as 0.70 °C over the northern hemisphere land, in contrast to the small cold bias of 0.02 °C in ACCESS1.3. The southern hemisphere land excluding Antarctica sees a larger warm bias in ACCESS1.3 (0.92 °C) than in ACCESS1.0 (0.26 °C). Such a contrast in the surface air temperature over land is mainly attributed to CABLE in ACCESS1.3 yielding significantly lower land surface albedo than MOSES in ACCESS1.0 (Kowalczyk et al. 2013).

Over the oceans, ACCESS1.3 is warmer than ACCESS1.0 in the northern hemisphere and the tropics but colder over the Southern Ocean. Particularly, ACCESS1.3 is 1.66 °C colder than ACCESS1.0 in high latitudes of the Southern

Table 2. The historical run present-day surface air temperature biases and RMSEs in ACCESS1.0 and ACCESS1.3 against the ERA-Interim reanalysis (Dee et al. 2011) data for 1979–2008. Values are presented for the groups of land and oceans, and for different zonal bands. (Units: °C).

	ACCESS1.0		*ACCESS1.3*		*ACCESS1.0 – ACCESS1.3*	
	Bias	*RMSE*	*bias*	*RMSE*	*Bias*	*RMSE*
All land	–0.38	1.96	0.14	2.21	–0.53	–0.25
0–90°N	–0.70	1.88	–0.02	2.12	–0.68	–0.24
60°S–0°	0.26	1.44	0.92	1.93	–0.66	–0.49
90°S–60°S	0.36	3.20	–0.53	3.25	0.89	–0.06
All oceans	–0.15	1.26	–0.06	1.40	–0.09	–0.13
60°N–90°N	–1.76	2.74	–1.16	2.73	–0.59	0.01
20°N–60°N	–0.51	1.17	–0.10	1.12	–0.41	0.05
20°S-20°N	–0.13	0.86	0.17	0.95	–0.30	–0.09
60°S–20°S	0.45	0.98	0.34	0.85	0.11	0.12
90°S–60°S	–0.99	2.52	–2.65	3.63	1.66	–1.11
Global	-0.21	1.48	–0.01	1.65	–0.20	–0.17

Ocean (>60°S). This is the effect of the larger sea-ice albedos used in ACCESS1.3, which overcompensate the cloud radiative forcing warming error shown in Fig. 6. It benefits ACCESS 1.3 by producing a greater sea-ice extent at the summer minimum, though leaves thick ice adjacent to the coast (see the 'Sea-ice' subsection and also Uotila et. al (2013) for more details).

Precipitation

Figure 4 shows the global maps of the present climate of precipitation from the ACCESS1.0 historical run, together with the observed climatology of precipitation and the model biases of the present climate from the historical runs. The two models simulate very similar global precipitation distribution patterns and intensities, both fairly close to the GPCP observation data (Huffman et al. 2009). The common model problem of a double intertropical convergence zone (ITCZ), which is seen in most of the IPCC AR4 models (e.g. Lin 2007) with excess rainfall simulated over the south side of the equator and reduction of rainfall over the other side, is still there weakly in the ACCESS models. Globally, ACCESS1.0 has a somewhat closer match to the observation than ACCESS1.3 in both the mean bias (0.39 vs. 0.42 mm/day) and RMSE (1.41 vs. 1.45 mm/day). Away from the tropical region, the models simulate excessive precipitation nearly everywhere; especially over the mid to high latitude oceans because of the dominant warm biases of SST there (see Fig. 14). In fact, the rainfall biases over the oceans are primarily determined by the SST biases, as evidenced by comparing the rainfall bias pattern shown here and the SST bias pattern shown in Fig. 14(c) and 14(d). For example, except for the tropical oceans, the regions with major warm biases (such as the oceanic frontal zones, the upwelling regions off the west coasts of South America and North America, but with the exception of South Africa) also have noticeable positive rainfall errors. Over the land, notable errors of excess precipitation are found over the Himalayas, southeast Africa, and the Andes in particular.

Total cloud amount and cloud radiative forcing (CRF)

One of the substantial differences between the ACCESS1.0 and the ACCESS1.3 atmospheric configurations is the cloud schemes. It is well recognised that clouds play a crucial role in modulating the climate with changes in the location or frequency of cloud distributions impacting both regional and global climate. This is because clouds constitute one of the major factors in determining the earth radiation budget, largely controlling the atmospheric circulation, hydrological cycle, and the surface energy budget (e.g. Stephens et al. 1990, Yao and Del Genio 1999, Williams et al. 2006, IPCC 2007). The uncertainty about the magnitude and sign of the cloud feedback on climate is considered one of the major obstacles in improving climate change prediction, and therefore improvements in the representation of clouds are an extremely challenging but crucial goal for climate and climate change modelling (e.g. IPCC, 2007). The availability of satellite observations for the past few decades provides a critical measurement of model performance in simulating cloud cover and cloud radiative forcing (CRF).

Figure 5 compares the modelled present day annual mean total cloud amount against the D2 ISCCP observations (Rossow and Schiffer 1999) for the period of 1983–2005. Both models simulate the global distribution patterns quite well. The highest cloud cover over the Tropical Warm Pool, Southern Ocean and North Atlantic Ocean are well captured, as are the minima over the subtropical desert regions. However, model deficiencies are evident and are different for ACCESS1.0 and ACCESS1.3 over various regions, as detailed by the two error maps and Table 3 which presents the modelled cloud amount biases and RMSEs over

Fig. 4. Precipitation climatology and biases: (a) GPCP precipitation (Huffman et al. 2009) 1979–2005 mean, (b) ACCESS1.0 present climate, (c) ACCESS1.0 biases, and (d) ACCESS1.3 biases. Units are mm/day.

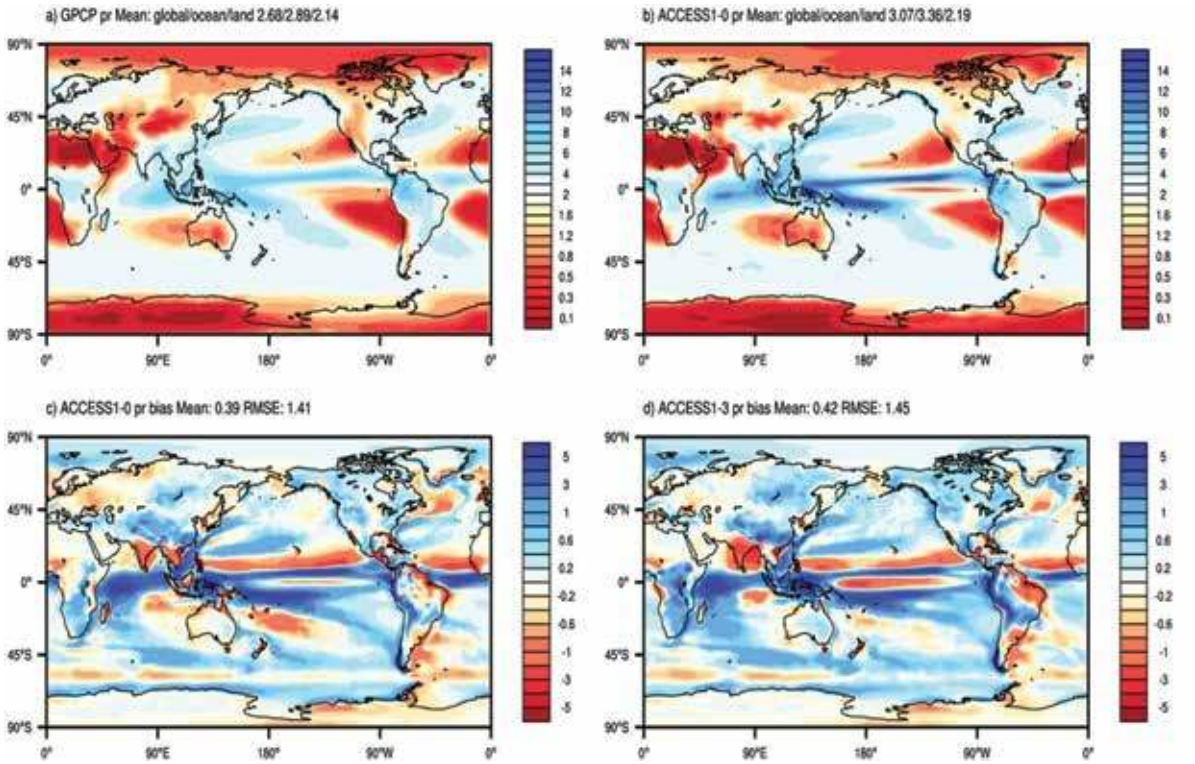

Table 3. Historical run present-day annual mean cloud amount biases and RMSEs in ACCESS1.0 and ACCESS1.3 against the D2 ISCCP observations for 1983–2005. Values are presented for different zonal bands and units are in per cent. Note the 60°–90° bands are excluded from the comparison because of the poor quality of observations in high latitudes.

	ACCESS1.0		*ACCESS1.3*		*ACCESS1.0 – ACCESS1.3*	
	Bias	*RMSE*	*Bias*	*RMSE*	*Bias*	*RMSE*
0–60°N	–13.8	15.6	–2.3	9.3	–11.5	6.3
60°S–0	–15.0	16.6	–4.8	10.6	–10.2	6.0
10°S–10°N	–13.9	15.7	2.6	10.8	–16.5	4.9
60°S–60°N	–14.4	16.1	–3.6	10.0	–10.9	6.1

different zonal bands. For ACCESS1.0, the globally averaged cloud fraction is 53.8 per cent, considerably lower than the ACCESS1.3 result which is 65.8 per cent, very close to the observed value of 66.5 per cent. The error in ACCESS1.0 results from the systematic underestimation of cloud cover between 60°N and 60°S, particularly the subtropical regions around 20°N and 20°S in the Indo-Pacific oceans where the largest underestimate is 30 per cent. For ACCESS1.3 the cloud cover error is noticeably more complicated. While the model generally underestimates cloud cover over the majority of the oceans between 60°S–60°N, it also overestimates cloud cover in parts of the tropics, with an average bias of 2.6 per cent within 10°S–10°N where ACCESS1.0 in contrast has an average cloud cover bias of –13.9 per cent. In polar regions, Fig. 5 shows that ACCESS1.3 overestimates cloud cover. However, ISCCP has significant uncertainties in these regions and Franklin et al. (2013) has shown that ACCESS1.3 cloud cover is in good agreement with CALIPSO observations in the high latitudes. Globally, ACCESS1.3 has a somewhat smaller RMSE than ACCCESS1.0, and the difference would be considerably enlarged when high latitudes are excluded from the calculation, as shown in Table 3. This indicates a significantly better simulation of cloudiness in ACCESS1.3 (with the PC2 cloud scheme) than in ACCESS1.0 (with the Smith cloud scheme).

CRF is a measure of how clouds affect the radiation budget at the top of the atmosphere and is calculated as the difference between the clear-sky and all-sky radiation. CRF influences surface heating gradients, and consequently can impact large-scale circulations and ocean heat transports. It is not only the total cloud cover that determines the CRF but also the vertical distribution of cloud, the condensate amount and the microphysical properties such as the effective radius. Figure 6 shows the short-wave, long-wave and net CRF errors

Fig. 5. Annual mean total cloud amount: (a) ISCCP climatology for 1983–2005, (b) ACCESS1.0 present-day climate, (c) ACCESS1.3 present-day climate, (d) ACCESS1.0 biases, and (e) ACCESS1.3 biases. Units are in per cent. Note that the ISCCP data has a notable discontinuity in the Indian Ocean because of a gap in coverage by geostationary satellites between Meteosat and GMS (Rossow and Garner 1993).

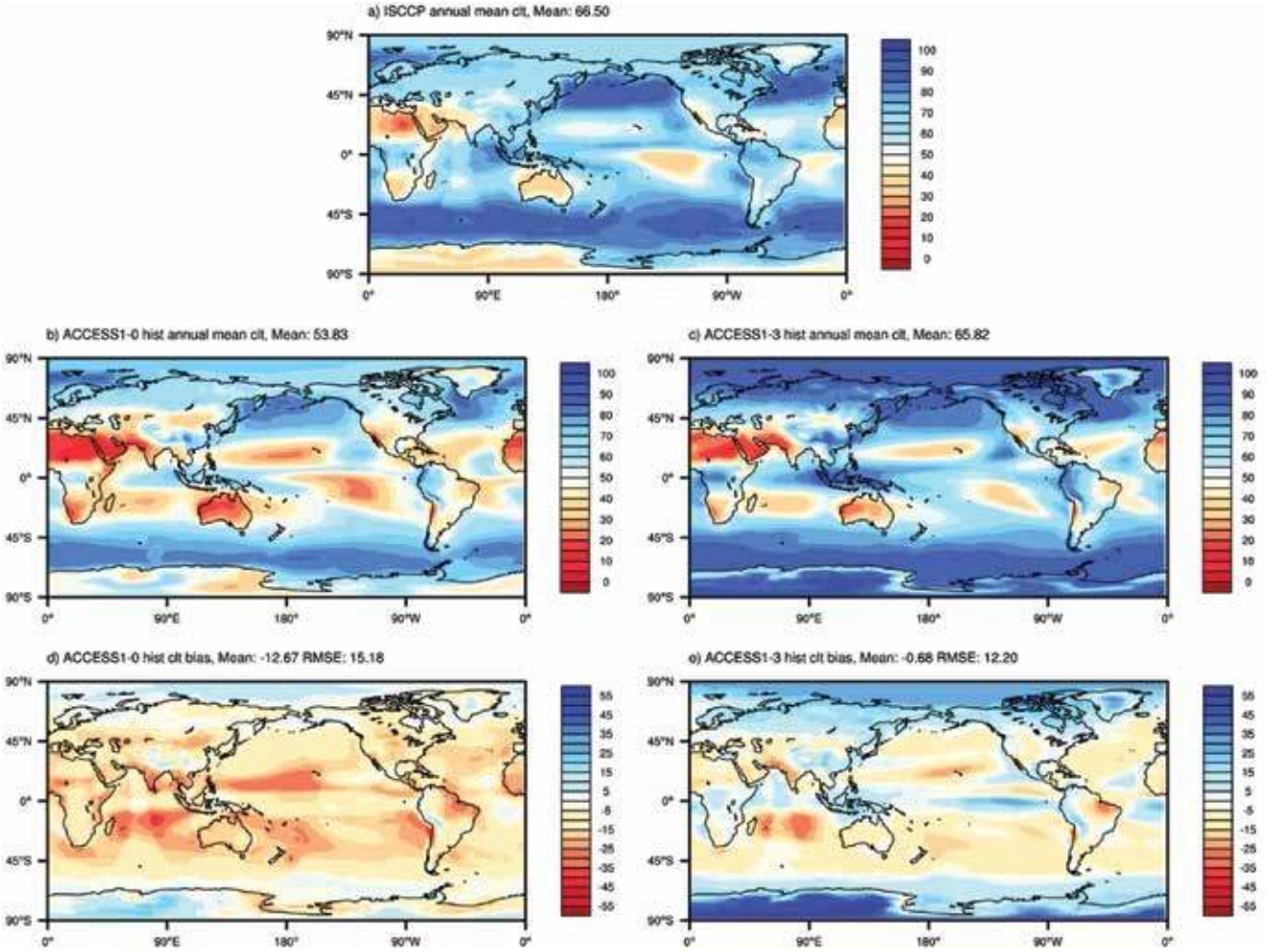

for ACCESS1.0 and ACCESS1.3 compared to the ISCCP observations. ACCESS1.3 simulates a global average annual mean total CRF of –17.9 W m^{-2}, weaker than the ACCESS1.0 result of –19.7 W m^{-2} which is closer to the observed value of –24.3 W m^{-2}. This is despite ACCESS1.0 simulating much less total cloud cover globally than the observations (Fig. 5) and demonstrates the importance of the cloud properties and vertical distribution of clouds for determining the CRF. The long-wave (LW) CRF is better simulated than short-wave (SW) CRF in both models in terms of the global mean error and spatial patterns. ACCESS1.3 has a smaller LW-CRF error than ACCESS1.0 in the tropics, suggesting that ACCESS1.3 has a better representation of the high clouds associated with deep convection. ACCESS1.3 shows larger SW-CRF errors than ACCESS1.0 over the Southern Ocean, particularly south of 60°S where the average SW CRF biases (over ocean) are 13.1 W m^{-2} and 5.5 W m^{-2} for ACCESS1.3 and ACCESS1.0, respectively. Given that Fig. 5 shows that ACCESS1.3 typically has higher cloud cover over the Southern Ocean, the weaker SW-CRF in ACCESS1.3 suggests that the clouds in this region are optically too thin. On the whole the total CRF errors are generally lower for ACCESS1.0 compared to ACCESS1.3 and this is partly due to better cancellation of errors between the SW-CRF and LW-CRF in ACCESS1.0, particularly in the tropics.

Model skill scores in simulating a selection of key fields

For a graphical depiction of skill in simulating the present climate, we adapt the histogram of skill scores of Gordon et al. (2010), following Watterson (1996). For each of 13 quantities and each of the four seasons, the global field from a model is compared to the best available observational field using the non-dimensional statistic M, as defined in the caption. The average of the four seasonal scores for each quantity is shown in Fig. 7, for each of three models. A value of one for M indicates perfect agreement, while zero indicates no skill. As can be seen each model produces considerable skill in each quantity. In most variables, in particular u500 and psl,

Fig. 6. Simulated annual mean cloud radiative forcing biases, relative to the ISCCP observations 1979–2008 mean, for short-wave (top panels), long-wave (middle panels) and total CRF (bottom panels). Left and right panels are for ACCESS1.0 and ACCESS1.3, respectively. Units are W m^{-2}.

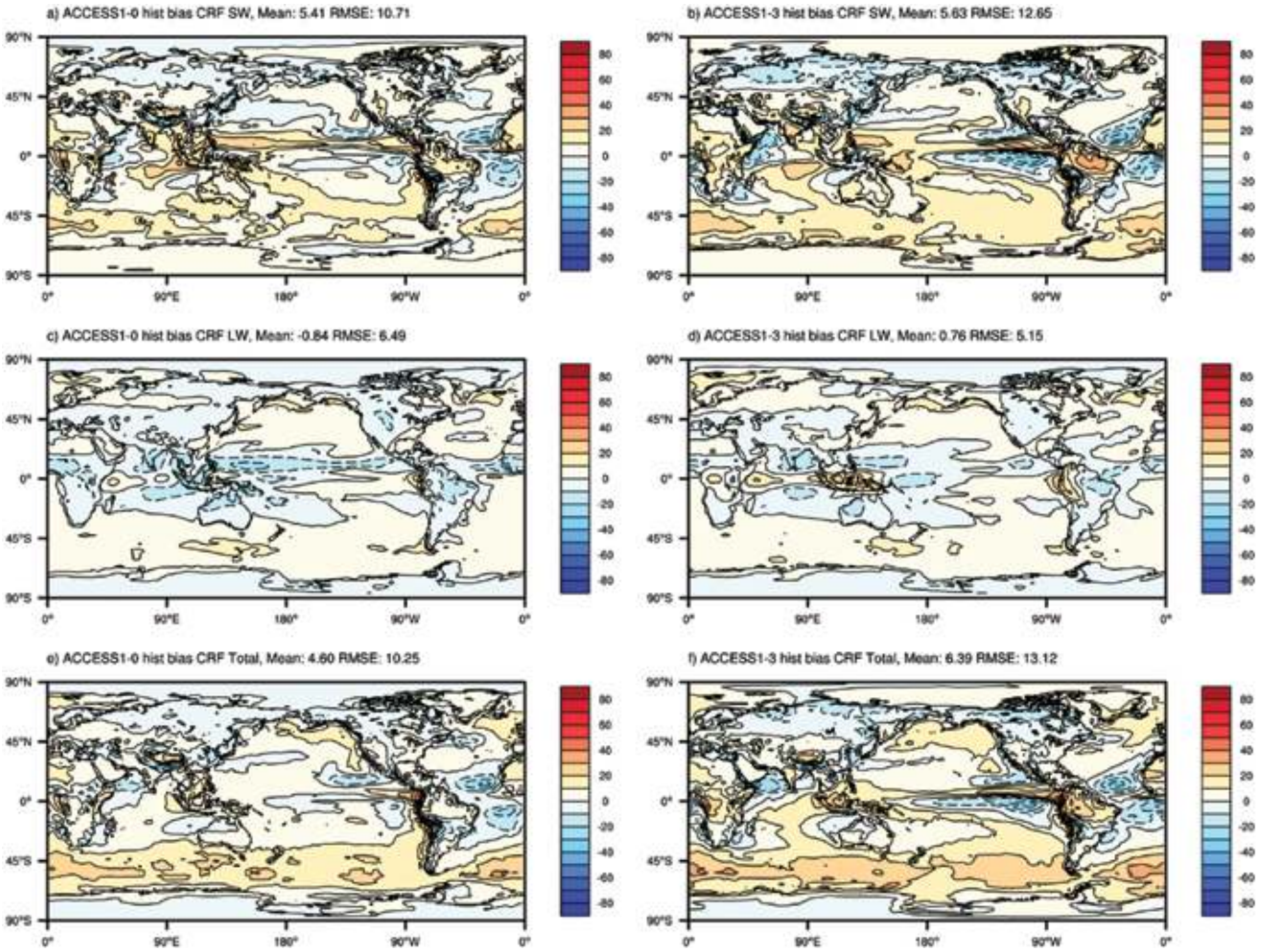

the ACCESS models provide a step up in skill compared to Mk3.5. Consistent with the RMSE values noted previously, ACCESS1.0 performed a little better than ACCESS1.3 for tas, pr and crf, but less well for clt. Averaging over the 13 variables gives M values of 0.77 for ACCESS1.0, 0.76 for ACCESS1.3 and 0.72 for Mk3.5.

The ACCESS model data are 30-year averages from the historical run, as above. The Mk3.5 fields are as in Gordon et al. (2010, from CMIP3 20C3M, 1961–90). For observations, we use here the ERA-interim data set (Dee et al. 2011), with ISCCP cloud (Rossow and Schiffer 1999) data as above. For the TOA quantities (rlut, rsut, crf), the fields are based on CERES satellite data over 2000–2005 provided by Pincus et al. (2008). As shown by Gordon et al. (2010), there is considerable uncertainty in the true climatologies, particularly for precipitation, cloud forcing and total cloud, which impacts on the scores. For further assessment of atmospheric circulations, see Rashid et al. (2013a).

Sea-ice

Time series of sea-ice extents and volume in the piControl runs

The sea-ice extent and volume time series from the ACCESS-CM piControl runs are shown in Fig. 8. The Arctic time series of ACCESS1.3 and ACCESS1.0 are relatively close, but in the Antarctic, the ACCESS1.3 sea-ice extent and volume are clearly higher than their ACCESS1.0 counterparts due to the effect of higher sea-ice albedo more than compensating for the larger CRF warming bias in ACCESS1.3 (Fig. 6(f)). The time series show large interannual and multi-decadal variability. ACCESS1.0 has a statistically significant 500-year sea-ice volume trend of –0.36 (–0.42) per cent/decade in the northern (southern) hemisphere. The corresponding ACCESS1.3 trends are –0.07 (+0.13) per cent/decade, which are also statistically significant, but clearly smaller than the ACCESS1.0 sea-ice volume drift. ACCESS1.0 is losing ice in both hemispheres, while ACCESS1.3 has hemispheric trends with opposite signs.

Ice coverage

The annual cycle of the sea-ice extent for the ACCESS1.0 and ACCESS 1.3 piControl runs is shown in Fig. 9. Modelled extents are rather close to the observed sea-ice extent climatology based on 1979–2005 monthly means. This indicates that the modelled sea-ice extents might be too small, especially in summer in the Arctic (Fig. 9(a)), because the climate during the historical period, used in the observations, is likely to be warmer due to the influence of greenhouse gas emissions than the piControl climate. On the other hand, the pre-industrial runs show a significant natural interannual variability having periods with temperatures similar to the historical era (Uotila et al. 2013). The impact of higher sea-ice albedo in the ACCESS1.3 simulation results in a systematic difference between the ACCESS1.3 and ACCESS1.0 sea-ice extent climatologies in the Antarctic (Fig. 9(b)), but not in the Arctic (Fig. 9(a)), where the location of land masses controls the sea-ice extent. A relatively low summer Arctic sea-ice extent could be due to the warm atmosphere and/or the ocean opening leads and polynyas in a thin ice field, which then enables the effective ice-albedo feedback process during the melting season and dominates

Fig. 7. The skill of models ACCESS1.0, ACCESS1.3 and Mk3.5 in reproducing observational climatological fields of various quantities. The bars give M scores for the global domain, averaged over four seasons, where $M = (2/\pi)\ arcsin\ [1 - mse / (V_X+V_Y + (G_X - G_Y)2)]$, with mse the mean square error between the model field X and observed field Y, and V and G are spatial variance and mean of the fields (as subscripted). The 13 fields presented here are: tas—surface air temperature; t500, u500, and r500—temperature, zonal wind and relative humidity, respectively, at 500 hPa; psl—sea level pressure; rsds—short-wave radiation down at surface; rlut, rsut, crf—long-wave radiation up, short-wave radiation up and cloud radiative forcing, respectively, at the TOA; prw—atmosphere water vapour content; pr—precipitation; evap—evaporation; clt—total cloud amount.

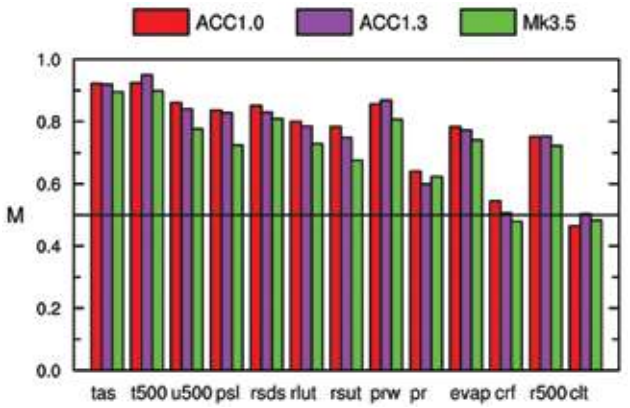

Fig. 8. The annual mean time series of ACCESS1.0 (red line) and ACCESS1.3 (blue line) piControl simulations for (a) Arctic and (b) Antarctic sea-ice extent, and for (c) Arctic and (d) Antarctic sea-ice volume. Sea-ice extent is defined as the area of grid cells comprising at least 15% of ice.

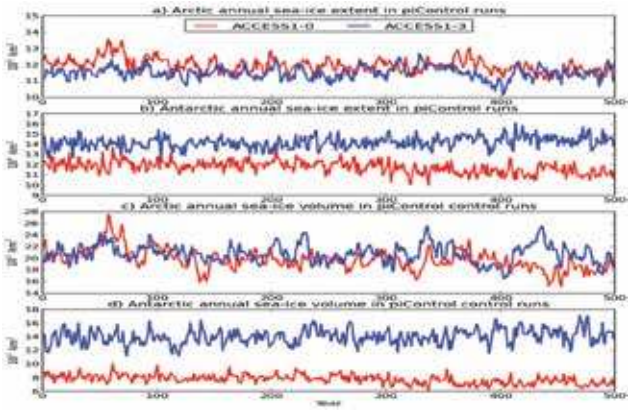

Fig. 9. Annual cycle of sea-ice extents for: (a) Arctic and (b) Antarctic. Black lines are the NSIDC observations for the 1979–2005 period, and red and blue lines are the piControl climatology (last 100-year mean) of ACCESS1.0 and ACCESS1.3, respectively. Units: 10^6 km^2.

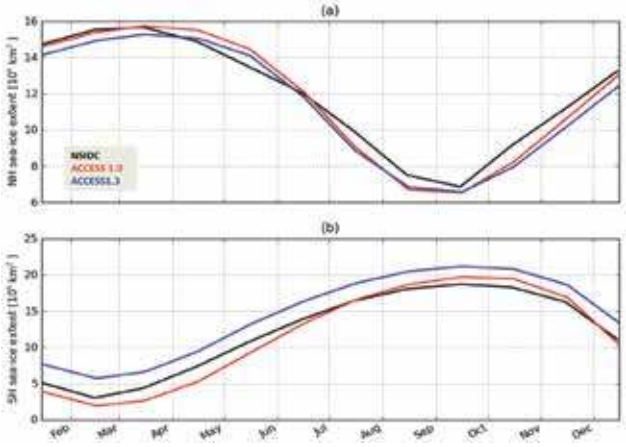

Fig. 10. Annual average sea-ice concentration of the last 100-year piControl simulations: (a) ACCESS1.0 Arctic, (b) ACCESS1.0 Antarctic, (c) ACCESS1.3 Arctic, and (d) ACCESS1.3 Antarctic. The 15% isoline of the observed SSMI sea-ice concentration for 1979–2000 is marked as a black continuous line.

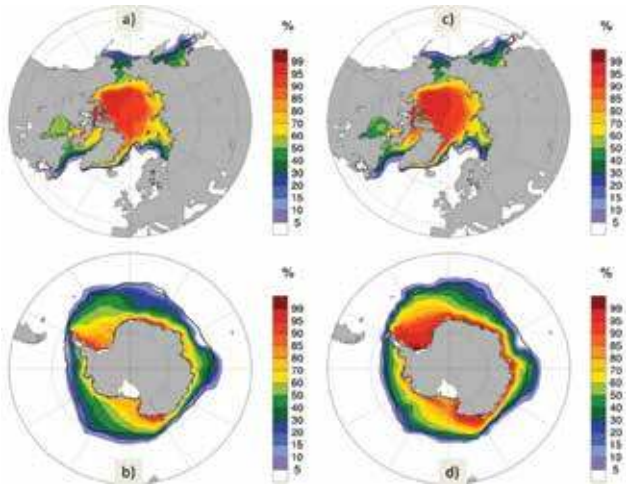

the annual cycle of the sea-ice thickness (Laxon et al. 2003), but it is not clear if this is the case in the model results.

Annual geographical mean sea-ice concentrations look reasonable and generally follow closely the observed 15 per cent sea-ice concentration isolines (Fig. 10). Additionally, the differences between the ACCESS1.0 and the ACCESS1.3 sea-ice concentration fields look small. In the Barents Sea, the ice edge in both ACCESS runs is too far north indicating that the ice is melting too much in summer. The ACCESS1.3 run seems to have a slightly larger area of very high sea-ice concentration of 99 per cent in the Central Arctic than the ACCESS1.0 run, probably due to the higher albedo. In the Antarctic, the simulated sea-ice edge is relatively close to the observed, which might indicate too small ice coverage for pre-industrial runs. The ACCESS1.3 ice concentration is clearly higher than the ACCESS1.0 ice concentration, and, as in the Arctic, this signifies the impact of the higher sea-ice albedo in the ACCESS1.3 simulation.

Fig. 11. The annual cycle of sea-ice volume averaged over last 100-year control simulations of ACCESS1.0 (red line) and ACCESS1.3 (blue line).

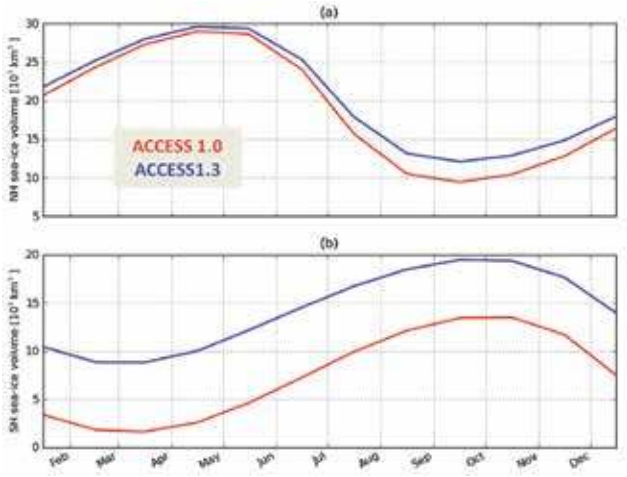

Fig. 12. Annual mean sea-ice thickness of the last 100-year piControl simulations: (a) ACCESS1.0 Arctic, (b) ACCESS1.0 Antarctic, (c) ACCESS1.3 Arctic, and (d) ACCESS1.3 Antarctic. The 15% isoline of the observed SSMI sea-ice concentration for 1979–2000 is marked as a black continuous line. Units: m.

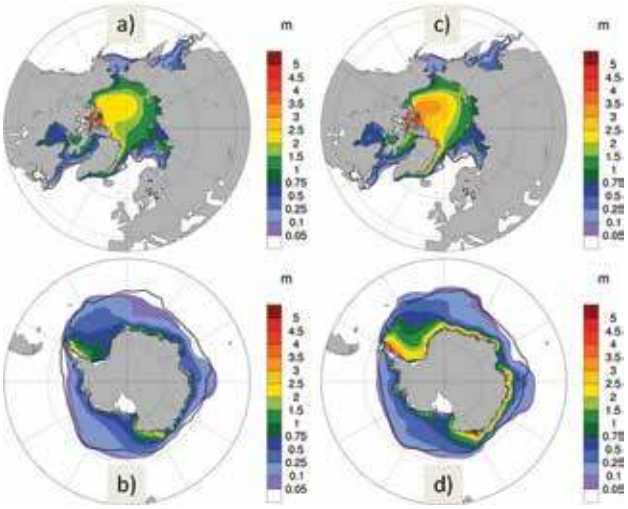

Ice thickness

The sea-ice volume between the ACCESS simulations (Fig. 11) is systematically higher in ACCESS1.3 than in ACCESS1.0 every month, which is not the case for the sea-ice extent (Fig. 10). This indicates the well known fact that the albedo impacts more on the sea-ice thickness than the sea-ice concentration (see for example Uotila et al. 2012), because the thinning of ice always reduces the ice volume, while the ice concentration decreases only after the ice has melted completely. Accordingly, the difference between the ACCESS1.0 sea-ice volume and the ACCESS1.3 sea-ice volume is larger during summer than in winter in both the Antarctic and the Arctic. As with the Antarctic sea-ice extent, ACCESS1.3 has a systematically higher sea-ice volume than ACCESS1.0, which indicates significantly thicker ice.

Figure 12 shows the annual mean sea-ice thickness of the last 100 years of the piControl simulations by ACCESS1.0 and ACCESS1.3. The thickest Arctic sea-ice in the ACCESS model appears in the narrow channels of the Canadian Arctic Archipelago, where air temperatures are cold and the ice is almost stationary. ACCESS1.0 has relatively thin ice, 2–2.5 m, in the Arctic Ocean north of Greenland, where ice thicknesses of 4–5 m have been observed (Fig. 12(a); Kwok and Cunningham 2008).The ACCESS1.3 ice is thicker north of Greenland, 3–4 m, but the relatively thick ice is transported by the strong anticyclonic Beaufort Gyre resulting in too thick ice in the central Arctic, while the ice is rather thin north of the Barents Sea close to the sea-ice edge.

In the Southern Ocean, the sea-ice is too thin especially in ACCESS1.0 (Fig. 12(b) and 12(d)). Close to the Antarctic continent, however, the sea-ice is thicker. Away from the Antarctic coast in the Southern Ocean, the ACCESS ice thickness is generally 0.1–0.5 m, which is less than observed (Worby et al. 2008), although the ACCESS1.3 sea-ice thickness looks more realistic than ACCESS1.0. The thin Antarctic ice suggests that the models do not simulate the deformation of ice due to rafting adequately in the Southern Ocean and/or the ice is melted by the oceanic heat (Uotila et al. 2012, Marsland et al. 2013).

Ocean

The oceans play a fundamental role in adjusting and stabilising the global climate. Ocean properties such as the sea surface temperature (SST) and salinity (SSS) are commonly used for model evaluation. The ocean surface thermohaline condition is the joint product of ocean thermodynamic and dynamic processes, along with ocean coupling to the overlying atmosphere and sea-ice (via heat, mass and momentum exchange) and land (river runoff input). The modelled evolutions of global mean SST (which is strongly coupled to the SAT over the open ocean) and

Fig. 13. (a) piControl time series of SST (in °C) , (b) piControl time series of sea surface energy budget (in W m^{-2}), (c) map of SST drift in ACCESS1.0, and (d) map of SST drift in ACCESS1.3. The time series is for global (sea surface) average annual mean, with thick lines being the linear regressions of the curves over the entire 500-year integration and the last 100-year period (green for ACCESS1.0 and cyan for ACCESS1.3). The maps of drift (°C) are for years 401–500 mean – years 1–100 mean.

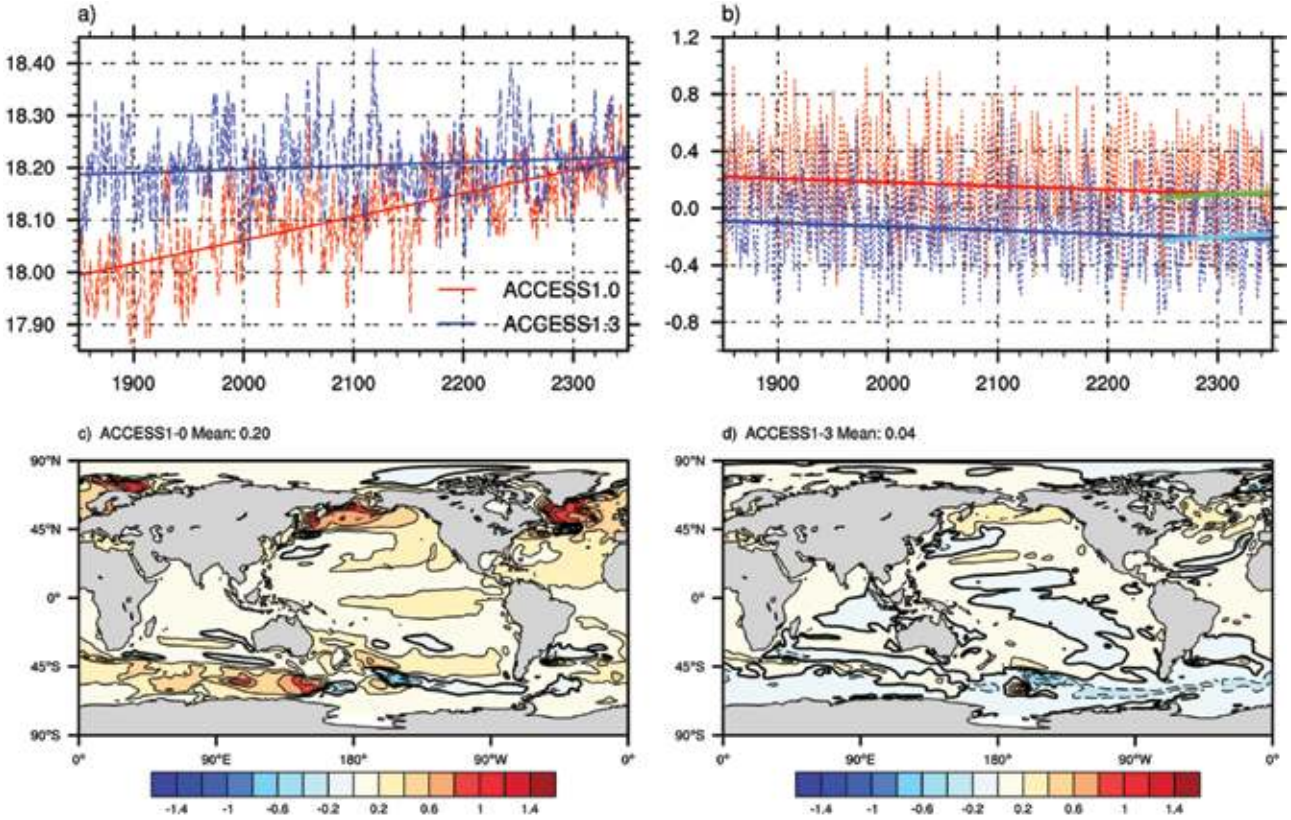

SSS demonstrate the climate stability, sensitivity, and, to a great degree, the reliability of a coupled model. The spatial distribution of the climatology and biases of SST and SSS provide a primary metric useful for evaluating model performance, including buoyancy and momentum fluxes, and surface currents.

Sea surface temperature

Figure 13(a) presents the annual mean global average SST evolution in the ACCESS-CM piControl simulations. As expected, SST evolves in a manner very similar to that of the SAT shown in Fig. 2(a). ACCESS1.0 has a small but noticeable trend in the control simulation with a final warming of about 0.42 °C and an average drift rate of 0.08 °C/century, and ACCESS1.3 holds a very stable sea surface equilibrium, with a nearly unnoticeable SST trend (<0.01 °C/century) throughout the control integration.

Figure 13(b) shows evolution of the ocean surface heat budget which consists of all the heat items (radiative and turbulent heat fluxes, ice formation-melt heat flux and precipitation associated heat flux), for the control runs of ACCESS1.0 and ACCESS1.3. Both models have a small but persistent imbalance of energy across the control integrations. The 500-year mean imbalances are only +0.15 and –0.15 W m^{-2} for ACCESS1.0 and ACCESS1.3, respectively, both being well below a traditional level of acceptance of ±1.0 W m^{-2} (e.g. Voldoire et al. 2012, Lucarini and Ragone 2011). These imbalances reflect the thermal adjustments occurring at the sea surface and in the ocean interior. For ACCESS1.0, this positive energy imbalance and the large warm biases found in the subsurface layers (see Marsland et al. 2013) jointly explain the lasting SST warm drift shown in Fig. 13(a). For ACCESS1.3, the continuous heat loss at the surface does not lead to a decrease in the global SST because, as in ACCESS1.0, the subsurface layers are overheated and the warm impact on the surface layer cancels and slightly outweighs the heat loss at the surface. It is noted that the trend of the ocean surface energy budget for the last 100-year has changed direction in the ACCESS1.3 case, indicating an improving heat balance for the ACCESS1.3 ocean.

Figures 13(c) and 13(d) show the SST drift maps for the two piControl runs using their last century average minus first century average. For ACCESS1.0 (Fig. 13(c)), the global mean SST change is just below 0.2 °C, but large regional drifts are evident in mid to high latitudes, and a maximum warming of about 1.4 °C is found in the northern hemisphere high latitude oceans. The Southern Ocean sees a maximum warming drift of nearly 1.0 °C south of Australia. The drifts in low latitudes are generally small. For ACCESS1.3 (Fig. 13(d)), the global mean warming drift is less than 0.04 °C, and there are no evident regional drift patterns in the world ocean. It is

Fig. 14. SST biases of: (a) ACCESS1.0 piControl climatology, (b) ACCESS1.3 piControl climatology, (c) ACCESS1.0 historical present climate, and (d) ACCESS1.3 historical present climate. For the piControl and historical biases, the reference data is the HadISST (Rayner et al. 2003) 1870–1899 SST reconstruction and the 30-year observation over 1976–2005, respectively. Units: °C.

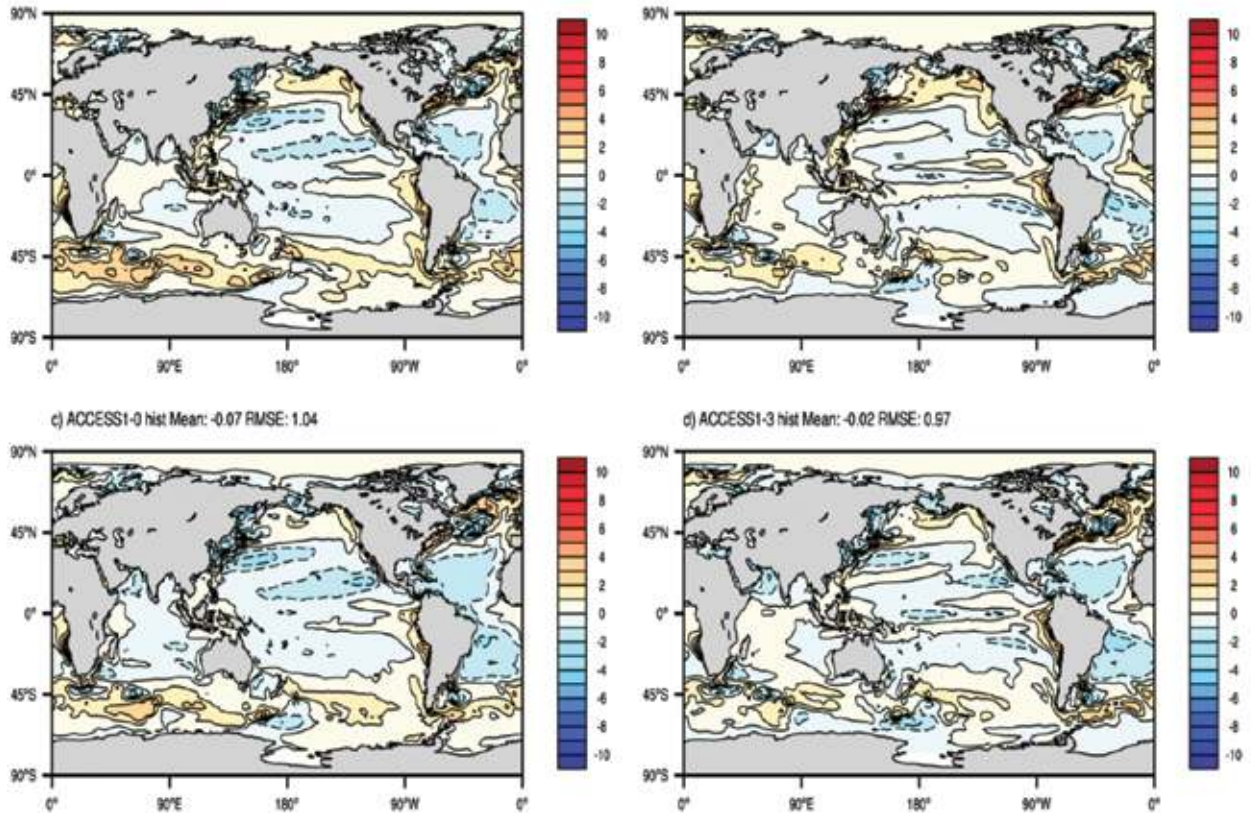

interesting to note that, while the low latitudes see nearly no SST trend at all in the 500-year run, the northern hemisphere high latitudes generally warm up, but the majority of regions in the Southern Ocean slightly cool down.

Figure 14 shows the SST biases of the ACCESS-CM piControl climate and historical present-day climates. We take the SST reconstruction for 1870–1899 from the HadISST dataset (Rayner et al. 2003) as the observation for the control runs to compare against. It is already noticed from Fig. 13(a) that the ACCESS1.0 piControl starts from a colder initial SST condition than ACCESS1.3 (by about 0.2 °C), warming up slowly in the course of the run, and catching up with ACCESS1.3 in the last 100 years of integration. Hence the two runs show similar SST piControl climatology, with global mean biases being about 0.25 °C and 0.26 °C, respectively. The RMS errors, 1.12 °C for ACCESS1.0 and 1.02 °C for ACCESS1.3, are moderate in both runs, but the difference indicates that ACCESS1.3 is in slightly better agreement with the observation, as evidenced by the details of the biases shown in Fig. 14(a) and 14(b). While the two runs have similar bias patterns nearly everywhere in the global ocean, ACCESS1.3 has larger areas than ACCESS1.0, where the biases are less than 1 °C, especially in the Pacific Ocean. Over the whole Southern Ocean, particularly the Indian Ocean section, the warming biases are significantly smaller in ACCESS1.3 than ACCESS1.0. As discussed above (i.e. the SAT subsection), this warming bias reduction is mainly attributed to the larger ice albedos used in ACCESS1.3, which result in much better simulation of the Antarctic sea-ice (as shown in the 'Sea-ice' subsection) and thus produce a more realistic SST near the Antarctic. However, ACCESS1.0 shows somewhat smaller cold biases in the tropical Pacific, which has important implications for the simulated ENSO behaviour (see Rashid et al. 2013b).

Apart from the above features, the two runs have comparable large biases in various regions. In the North Atlantic, for example, the cold error southeast of the Labrador Sea and the adjoining warm errors to the south are associated with a poor representation of the Gulf Stream path (too far south) and the model's inability to explicitly resolve eddy transports. As pointed out by Griffies et al. (2011), this region, as well as some other major frontal zones such as the North Pacific western boundary current (Kuroshio Current), has strong SST gradients, and small errors in the simulated flow location and intensity can lead to large SST errors. In addition, broad cooling biases are evident at both sides of the equator in the Atlantic Ocean, mainly attributed to the model producing too strong SW cloud radiative forcing there, as shown in Fig. 6. This is the case for both ACCESS1.0 and ACCESS1.3.

Fig. 15. Time series of annual mean global average: (a) SSS (in psu), and (b) P–E+R (in mm/year) at the ocean surface, from the ACCESS1.0 (red) and ACCESS1.3 (blue) piControl runs. Also presented in (b) are the linear regressions (thick lines) of the water budgets over the entire 500-year integration and the last 100-year period (red/green for ACCESS1.0 and blue/cyan for ACCESS1.3).

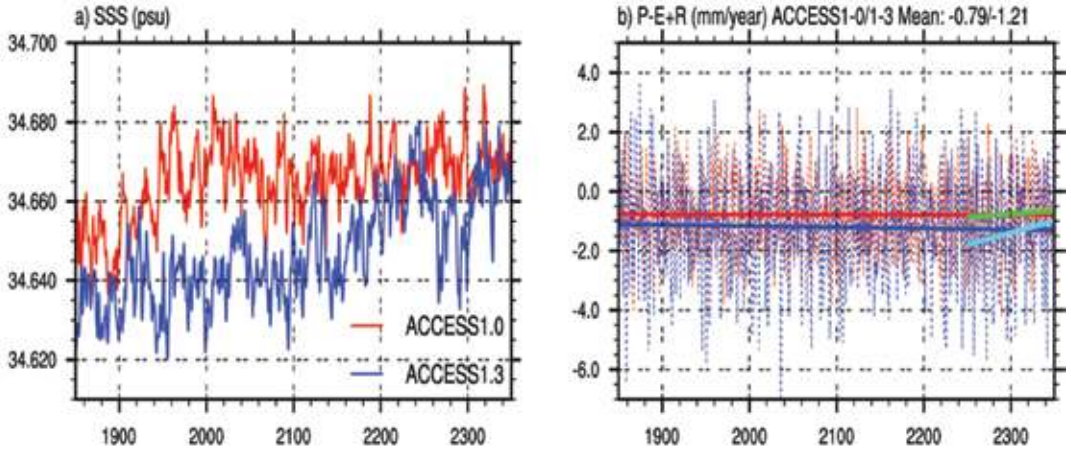

Another apparent deficiency seen from the bias maps is the warming bias off the west coast of America and Africa. As shown by Griffies et al. (2009), this is an intrinsic deficiency shared by nearly all state-of-the-art ocean models, most likely attributable to the model underestimating the upwelling and associated westward mass transport due to the coarse resolution of the model grids in both the ocean and atmosphere.

All the major features of the piControl SST biases discussed above also appear in the historical present-day climate, as shown by Fig. 14(c), 14(d). Again, ACCESS1.3 has significantly less warm biases in the Southern Ocean but broader cold biases across the equatorial Pacific Ocean than ACCESS1.0. While the other major similarities and differences between the pair of control runs are well reflected in the historical runs, the global mean biases (–0.072 °C and –0.016 °C) and the RMS errors (1.04 °C for ACCESS1.0 and 0.96 °C for ACCESS1.3) are mostly reduced, partly attributed to the noticeable reduction of warming over the North Pacific region. This may be associated with the impact of aerosol forcing which cools the surface temperature and thus enhances the cold biases, particularly in the northern hemisphere, as evidenced in these SST bias maps.

Sea surface salinity

Figure 15(a) shows the evolution of annual mean globally averaged SSS through the piControl runs. ACCESS1.3 has an apparent increase of SSS, with interannual and decadal variations, over the course of the piControl simulation. This drift suggests the ocean recovering from a 'coupling shock' (not shown) which brings the global mean SSS down to a minimum of 34.57 psu from the initial value of around 34.72 psu within the first 50 years of the spin-up integration. The global SSS then starts rising and takes 200 years to reach a level of about 34.63 psu when the piControl simulation starts. The 250-year spin-up for the model is far from enough to stabilise the global mean SSS. It still has the appearance of ongoing 'recovery' through at least the first 400 years of the piControl integration. Note one may not expect prefect equilibrium for the global mean SSS because of the imbalance of fresh water budget at the ocean surface, as shown in Fig. 15(b). ACCESS1.0 experiences a similar sudden freshening in the early stage of its 300-year spin-up, but the global mean SSS recovers much faster than that in ACCESS1.3, and appears to reach a quasi-equilibrium within 100 years of the start of the piControl simulation. Fig. 15(b) presents the freshwater budget (precipitation – evaporation + runoff) at the global ocean surface. The overall very minor negative imbalance of water flux (~0.1 mm/year) has little association with the SSS evolution, but it has direct impact on the global ocean sea level and the volume-average salinity, as discussed below. Note that, like the energy budget trend shown in Fig. 13(b), the water imbalance is evidently improving during the last 100-year simulation, as indicated by the change in trend for this period.

Figure 16 shows the spatial distributions of the historical run present day SSS biases relative to the WOA2009 data (Antonov et al. 2010). The two models have a similar global bias pattern. The pattern is very similar to what was found in the GFDL CM2.1 and CM3 models (Griffies et al. 2011). Large fresh biases are located in the eastern Mediterranean Sea, east Asian marginal seas, North Sea, Baltic Sea and Gulf of Bothnia, and particularly Hudson Bay. These extreme fresh biases are possibly associated with river routing errors in the land surface model and also due to the difficulty in a coarse resolution model of representing the circulation in an enclosed basin with limited connection to the open ocean. In the North Atlantic, a fresh bias is found off Newfoundland. This freshening bias, along with the corresponding cooling bias discussed earlier, is associated with the model's deficiency in representing the Gulf Stream path which in reality turns east at higher latitudes so that the warm, salty waters from low latitudes are transported into the northern North Atlantic. Over other regions, large positive salinity

Fig. 16. Historical run present-day annual mean SSS biases (model – WOA2009 data): (a) ACCESS1.0, and (b) ACCESS1.3. Units: psu.

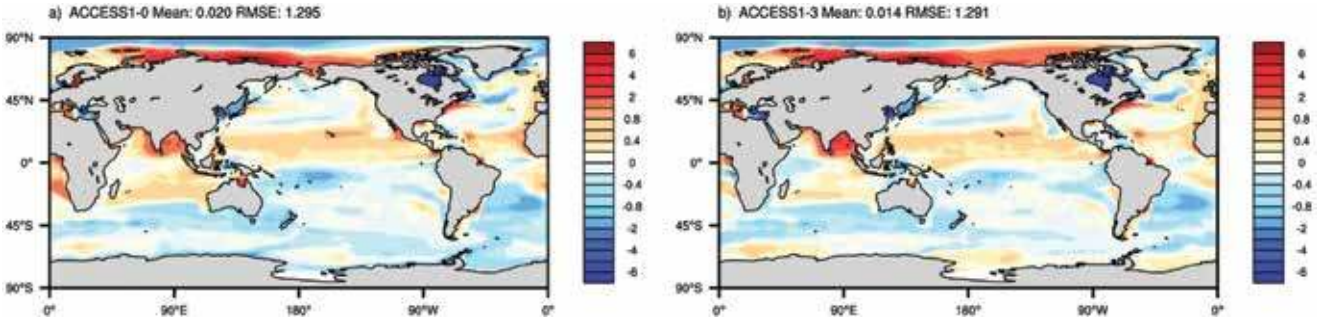

Table 4. Historical run present-day SSS biases and RMSEs in ACCESS1.0 and ACCESS1.3 against theWOA2009 data. Values are presented for selected zonal bands and global mean. (Units: psu). Note the underlined numbers are for comparison with the GFDL CM3 model results (Griffies et al. 2011).

	ACCESS1.0		*ACCESS1.3*		*RMSE excluding Hudson Bay and Gulf of Bothnia*	
	Bias	*RMSE*	*Bias*	*RMSE*	*ACCESS1.0*	*ACCESS1.3*
70°N–90°N	1.324	3.066	1.532	3.001		
30°N–70°N	–0.436	2.678	–0.461	2.689	1.199	1.211
30°N–90°N	**–0.127**	**2.750**	**–0.114**	**2.746**	**1.690**	**1.677**
0-30°N	0.423	0.773	0.403	0.823		
30°S–30°N	**0.216**	**0.686**	**0.163**	**0.687**		
30°S–0	0.021	0.593	–0.062	0.529		
90°S–30°S	**–0.236**	**0.441**	**–0.172**	**0.414**		
Global	0.020	1.295	0.015	1.291	0.902	0.894

biases are found in several places. A large salinity error is located in the Arctic Ocean (north of Siberia), likely resulting from poor representation of river runoff in the atmosphere-land component and a summer bias in the observational data in ice covered waters. Also notable is the large area of high salinity errors in the Arabian Sea and the Bay of Bengal, which is associated with the negative rainfall bias there, as shown in Fig. 4(c) and 4(d). In the tropical oceans the SSS biases are also largely determined by the rainfall errors. The small area of strong bias (up to 20 psu) located off northeast South America is attributed to the weak outflow of the Amazon River.

Table 4 summarises the simulated present-day SSS biases and RMSEs in ACCESS1.0 and ACCESS1.3 against the WOA2009 data for different zonal bands and global mean. The models have the largest SSS biases and RMSEs in the Arctic Ocean and the smallest SSS errors in the southern tropical oceans. The globally averaged SSS biases are 0.020 psu for ACCESS1.0 and 0.015 psu for ACCESS1.3, respectively, indicating a reasonable match of the simulated SSS to the observations. However, the RMS errors, over 1.29 psu for both models show large spatial deviation of the modelled distributions from the observations. Such large RMS errors are due to the extreme, localised biases mentioned above. In fact, excluding extreme freshening of more than 8 psu (i.e. in Hudson Bay and Gulf of Bothnia) alone would have the SSS RMS errors significantly reduced (see the last two columns of Table 4). For the three zonal bands highlighted in Table 4, the two ACCESS models show RMS errors comparable to the GFDL CM3 results presented by Griffies et al. (2011), except the northern band where ACCESS-CM has larger salinity errors in the Arctic Ocean.

Ocean interior properties

The ocean is spun up from present-day temperature and salinity conditions with preindustrial atmospheric forcing, and such an approach requires thousands of years of integration for the ocean interior, particularly the deep ocean to reach its equilibrium (e.g. Stouffer 2004). Because of our very short spin-up periods (i.e. 300 years for ACCESS1.0 and 250 years for ACCESS1.3), it is unsurprising that during the 500-year control simulation the models show trends in the evolution of the ocean interior. Fig. 17 displays the time series of global ocean volume-averaged temperature and salinity in the control runs.

Both model versions undergo slow and steady changes of the water properties, but the drifts are in opposite directions. While ACCESS1.0 is persistently warming up with an average rate of 0.03 °C/century, ACCESS1.3 is cooling down at a similar rate, resulting in a thermal deviation of 0.45 °C

Fig. 17. piControl run annual mean global ocean volume-averaged evolution of (a) temperature (°C), and (b) salinity (psu). Red for ACCESS1.0 and blue for ACCESS1.3.

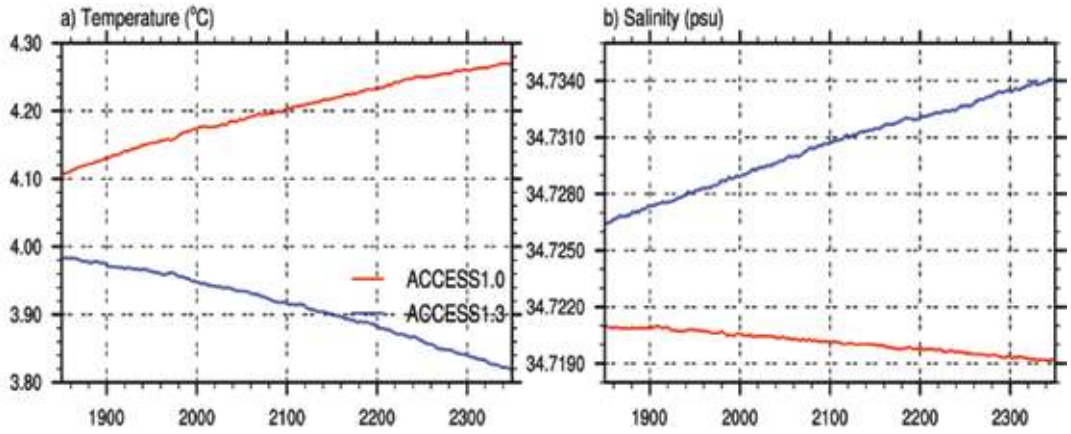

between the two model oceans by the end of the piControl runs (including the initial difference of 0.13 °C at the end of the spin-up phase). Such contrasting thermal evolutions are attributed to the different surface energy budgets achieved for the two models. As shown in Fig. 13(b), whereas the ACCESS1.0 ocean sees a net energy gain and therefore warms up, the ACCESS1.3 ocean is losing heat and thus cools down. In fact, at the early stage of spin-up (not shown), both models are evidently warming up due to a large energy imbalance at the TOA which results in a net energy gain into the ocean. As described in the 'Experimental design' section, since year 150 in the spin-up phase (when the global ocean is warmed to about 4 °C from an initial temperature of 3.67 °C), ACCESS1.3 uses larger sea-ice albedos (Table 1) to produce a more realistic climate. This results in a much smaller energy imbalance at the TOA, and the heat exchange at the ocean surface reaches a temporary balance which lasts for a few decades. Then the surface heat budget changes sign (from net gain to net loss), and the ocean starts cooling down. This cooling continues in the piControl run, as seen in Fig. 17(a). One may expect that this ocean cooling will gradually slow down following the evolution of the ocean surface heat budget as shown in Fig. 13(b). In the ACCESS1.0 case, with a large positive heat budget at the TOA, the ocean surface never achieves an energy balance as seen in ACCESS1.3, and the ocean warming remains through the spin-up integration and then the whole control run.

The global ocean warming or cooling signal found in the two models is not uniform in distribution. These trends are the net effect of complicated temperature changes within ocean basins and on isopycnal surfaces. Taking the zonal mean, depth dependent features (not shown, see Marsland et al. 2013) as an example, both models have slow but prolonged cooling throughout the water column in the Southern Ocean (south to 60°S), and this cooling spreads northwards into the global deep ocean below 2000 m via a strong Southern Ocean abyssal cell. Meanwhile, the top layers (above 2000 m, north to 60°S), particularly the 200–1500 m layer, see considerable warming. For ACCESS1.0, the deep ocean cooling is outweighed by the top layer warming, resulting in an overall warming drift shown in Fig. 17(a). The opposite situation is seen in ACCESS1.3 which shows an overall cooling drift in the ocean. This trend in the ocean interior is also found in the ACCESS-OM benchmarking experiment (Bi et al. 2013).

For the piControl run global ocean volume-averaged salinity, ACCESS1.0 shows a weak decrease whilst ACCESS1.3 undergoes a considerable increase. Examination of the ocean surface fresh water budget (Fig. 15(b)) reveals that both models are losing water. With a loss rate of 0.121 mm/year, ACCESS1.3 has a sea level decrease of 60.5 cm by the end of the 500-year piControl, which largely, but not completely, explains the salinity increase of about 0.007 psu seen in Fig. 17(b). In fact, with the model's volume conserving configuration (excluding change associated with the surface mass fluxes of freshwater), an increase of 0.00756 psu (from 34.7265 psu to 34.7341 psu) in the global ocean salinity indicates a water volume decrease of 2.896×10^{14} m^3, equivalent to a sea level drop of 80.1 cm. In the ACCESS1.0 case, however, the global ocean is freshening throughout the piControl run, despite the ocean surface budget showing a net loss of water (39.2 cm/500 years) from the ocean. These mismatches indicate some unknown leak of water in ACCESS1.3 but a spurious source of water in ACCESS1.0, requiring further investigation. The differences in the non-conservation of hydrology between ACCESS1.0 and ACCESS1.3 impede the diagnosis of the models sea level as discussed in Marsland et al. (2013) and require further investigation.

Summary and conclusion

This paper documents the ACCESS-CM, a new coupled climate model developed at the Centre for Australian Weather and Climate Research, a partnership between CSIRO and the Bureau of Meteorology. Two versions of this model, ACCESS1.0 and ACCESS1.3, have been used in

parallel to conduct a set of CMIP5 experiments, and basic evaluation has been performed in this study based on the 500-year preindustrial control integrations and 156-year historical simulations (from 1850 to 2005) in comparison with observations or reanalysis estimations whenever applicable. Results of all the ACCESS-CM CMIP5 experiments have been made available to the international community[10] for model intercomparison studies within the CMIP5 framework.

The basic evaluation of model performance presented in this paper shows that, despite some deviations, the two versions of ACCESS-CM generally simulate similar global average annual mean climate under both preindustrial and the reconstructed historical atmospheric forcing conditions, and the results are either close to the available observations/reanalysis estimations or comparable to the results of other CMIP5 models (see e.g. Watterson et al. 2013). For the preindustrial control simulations, ACCESS1.3 shows nearly no drift in the global average annual mean surface air temperature while ACCESS1.0 has a weak warming trend of 0.07 °C/century. The drift found in the ACCESS1.0 piControl has very limited effect on the climate change signals simulated in the historical and RCP forcing scenario runs (Dix et al. 2013). The deep ocean shows significant long term drifts in both temperature and salinity, which persist through the course of the 500-year piControl simulation, and which will need to be taken into account when using the model output in analysis such as for sea level change. As shown by Dix et al. (2013), the historical simulations also successfully capture the major features of the observed SAT evolution, especially the rapid warming epoch of the past few decades. In addition, the ACCESS-CM model skill scores in simulating the present climate of a selection of key atmospheric quantities, globally and over Australia (Watterson et al. 2013), significantly surpass that of the preceding CSIRO Mk3.5 model delivered to IPCC AR4.

Because of the substantial difference in their atmosphere-land surface configurations and a few different parameters used for the ice and ocean, evident distinctions between the two models are found in some of the simulated fields, in terms of both global mean and geographical distribution. For example, ACCESS1.3 produces a higher global mean SAT than ACCESS1.0, which is largely attributed to the lower land surface albedo from the CABLE model over majority of the continents (see Kowalczyk et al. 2013) that results in a considerably warmer land surface condition. Another example is that the PC2 scheme (ACCESS1.3) shows significant improvement over the Smith scheme (ACCESS1.0) in simulating the global cloud coverage, particularly in the tropics (Fig. 5, also see Franklin 2013). However, this does not necessarily lead to a corresponding improvement in the cloud radiative forcing. In fact, the solar CRF and therefore the total CRF simulated by ACCESS1.3 are overall poorer than that by ACCESS1.0, particularly over the Southern Ocean.

Both ACCESS1.0 and ACCESS1.3 yield solutions which overall show significant improvement over those for the Australian CMIP3 contributions. Nevertheless, the models and their solutions possess certain imperfections, as discussed previously. Since the CMIP5 simulations were performed, a program of model testing and development has continued to address these imperfections. The primary focus is on improvements to ACCESS1.3 which, with its inclusion of CABLE and the first of the GA series of atmospheric components, is the preferred model for a range of activities undertaken by the Australian climate research community, and a starting point for development of the next generation of model for application beyond CMIP5.

[10]The ACCESS raw model outputs have been written out to CMIP5 specifications that include 1) providing many of the requested parameters, 2) following the Data Reference Syntax and Controlled Vocabularies, i.e. file and directory naming conventions, and 3) ensuring metadata contained in the requested netCDF files following specified conventions such as CMIP5 experiment instructions (Taylor et al. 2011). Datasets that pass the CMIP5 quality control standards have been published to the Earth System Grid (ESG) and available to the international community via the CMIP5 data portal.

Acknowledgments

This work has been undertaken as part of the Australian Climate Change Science Program, funded jointly by the Department of Climate Change and Energy Efficiency, the Bureau of Meteorology and CSIRO. The computation for this work was performed at the NCI National Facility at the Australian National University, and we particularly thank Dr Ben Evans and the other NCI staff members for their support. We further thank Cath Senior, Chris Gordon and Gill Martin of the Met Office for helpful discussions during the course of this work, and Gill Martin and Charline Marzin for HadGEM and proto-HadGEM3 model output fields useful for comparison and benchmarking. We thank Leon Rotstayn for his comments on a pre-submission draft. We finally thank other members of CAWCR and the Australian Research Council Centre of Excellence for Climate System Science who have contributed their views and encouragement during the course of this work.

References

Adcroft, A. and Campin, J.-M. 2004. Rescaled height coordinates for accurate representation of free-surface flows in ocean circulation models. *Ocean Modell., 7,* 269–284.

Adcroft, A., Hill, C., Marshall, J. 1997. Representation of topography by shaved cells in a height coordinate ocean model. *Mon. Weather Rev., 125,* 2293–2315.

Antoniou, J., Locarnini, R., Boyer, T., Mishonov, A., Garcia, H. 2006. *World Ocean Atlas 2005*, Volume 2: Salinity. U.S. Government Printing Office 62, NOAA Atlas NESDIS, Washington, DC, 182 pp.

Antonov, J.I., Seidov, D., Boyer, T.P., Locarnini, R.A., Mishonov, A.V., Garcia, H.E., Baranova, O.K., Zweng, M.M., and Johnson, D.R. 2010. *World Ocean Atlas 2009*, Volume 2: Salinity. S. Levitus, Ed. NOAA Atlas NESDIS 69, U.S. Government Printing Office, Washington, D.C., 184 pp.

Arakawa, A. and Lamb, V.R. 1977. Computational design and the basic dynamical processes of the UCLA general circulation Model. *Methods in Computational Physics, 17,* p173.

Arribas, A., Glover, M., Maidens, A., Peterson, K., Gordon, M., MacLach-

lan, C., Cusack, S., and Scaife, A. 2011. The GloSea4 ensemble prediction system for seasonal forecasting. *Mon. Weather Rev., 139,* 1891–1910. doi: 10.1175/2010MWR3615.1

Avila, F.B., Pitman, A.J., Donat, M.G., Alexander L.V., and Abramowitz, G. 2012. Climate model simulated changes in temperature extremes due to land cover change, *J. Geophys. Res., 117,* D04108, doi:10.1029/2011JD016382.

Bellouin, N., Rae, J., Jones, A., Johnson, C., Haywood, J., and Boucher, O. 2011. Aerosol forcing in the Climate Model Intercomparison Project (CMIP5) simulations by HadGEM2-ES and the role of ammonium nitrate. *J. Geophys. Res., 116,* D20206, doi:10.1029/2011JD016074.

Bi, D. and Marsland, S.J. 2010. Australian Climate Ocean Model (AusCOM) Users Guide. *CAWCR Technical Report No. 027*, The Centre for Australian Weather and Climate Research, a partnership between CSIRO and the Bureau of Meteorology. 72 pp. ISBN: 978-1-921605-92-5 (PDF).

Bi, D., Marsland, S.J., Uotila, P., O'Farrell, S., Fielder, R., Sullivan, A., Griffies, S.M., Zhou, X., and Hirst, A.C. 2013. ACCESS OM, the Ocean-Sea Ice Core of the ACCESS Coupled Model. *Aust. Met. Oceanogr. J.*, 63, 213–232.

Boutle, I.A. and Morcrette, C.J. 2010. Parametrization of area cloud fraction. *Atmos. Sci. Let., 11,* 283–289.

Cai, W., Sullivan, A., and Cowan, T. 2009. Climate change contributes to more frequent consecutive positive Indian Ocean Dipole events. *Geophys. Res. Lett., 36,* L19783, doi:10.1029/2009GL040163.

Collins, M., An, S-I., Cai, W., Ganachaud, A., Guilyardi, E., Jin, F-F., Jochum, M., Lengaigne, M., Power, S., Timmermann, A., Vecchi, G. and Wittenberg, A. 2010. The Impact of Global Warming on the Tropical Pacific and El Niño. *Nature Geoscience, 3,* 391–397.

Collins, W.J., Bellouin, N., Doutriaux-Boucher, M., Gedney, N., Hinton, T., Jones, C.D., Liddicoat, S., Martin, G., O'Connor, F., Rae, J., Senior, C., Totterdell, I., Woodward, S., Reichler, T., Kim, J., Halloran, P. 2008. Evaluation of the HadGEM2 model. Hadley Centre Technical Note HCTN 74, Met Office Hadley Centre, Exeter, U.K.,http://www.metoffice.gov.uk/learning/library/ publications/science/climate-science.

Cox, P., Betts, R., Bunton, C., Essery, P., Rowntree, R. and Smith, J. 1999. The impact of new land surface physics on the GCM simulation of climate and climate sensitivity. *Clim. Dyn., 15,* 183–203.

Davies, T., Cullen, M.J.P., Malcolm, A.J., Mawson, M.H., Staniforth, A., White, A.A., and Wood, N. 2005. A new dynamical core for the Met Office's global and regional modelling of the atmosphere. *Q. J. R. Meteorol. Soc., 131,* 1759–1782.

Dee, D.P., Uppala, S.M., Simmons, A.J., Berrisford, P., Poli, P., and others. 2011. The ERA-Interim reanalysis: configuration and performance of the data assimilation system. *Q. J. R. Meteorol. Soc., 137,* 553–597.

Dix, M., Vohralik, P., Bi, D., Rashid, H., Marsland, S.J., O'Farrell, S., Uotila, P., Hirst, A.C., Kowalczyk, E., Sullivan, A., Yan, H., Franklin, C., Sun, Z., Watterson, I., Collier, M., Noonan, J. Rotstayn, J. Stevens, L., Uhe P., and Puri, K. 2013. The ACCESS Coupled Model: Documentation of core CMIP5 simulations and initial results. *Aust. Met. Oceanogr. J., 63,* 83–99.

Dunne, J.P., John, J.G., Adcroft, A.J., Griffies, S.M., Hallberg, R.W., Shevliakova, E.N., Stouffer, R.J., Cooke, W., Dunne, K.A., Harrison, M.J., Krasting, J.P., Levy, H., Malyshev, S.L., Milly, P.C.D., Phillipps, P.J., Sentman, L.A., Samuels, B.L., Spelman, M.J., Winton, M., Wittenberg, A.T., and Zadeh, N. 2012 GFDL's ESM2 global coupled climate-carbon Earth System Models Part I: Physical formulation and baseline simulation characteristics. *J. Climate*, 25, 6646–6665. doi:10.1175/JCLI-D-11-00560.1.

Durack, P.J., Wijffels S.E., and Matear, R.J. 2012. Ocean Salinities Reveal Strong Global Water Cycle Intensification During 1950 to 2000. *Science*, *336*, 455–458. DOI: 10.1126/science.1212222.

Edwards, J.M., Beare, R.J., and Lapworth, A.J. 2006. Simulations of the observed evening transition and nocturnal boundary layers: Single-column modelling. *Q. J. R. Meteorol. Soc., 132,* 61–80.

Edwards, J.M. and Slingo, A. 1996. Studies with a new flexible radiation code. I: Choosing a configuration for a large-scale model. *Q. J. R. Meteorol. Soc, 122,* 689–720.

Elliott, S.M., Deal, C., Humphries, G., Hunke, E.C., Jeffery, N., Jin, M., Levasseur, M., and Stefels, J. 2012. Pan-Arctic simulation of coupled nutrient-sulfur cycling due to sea ice biology: Preliminary results, *J. Geophys. Res., 117,* 1–16, doi:10.1029/2011JG001649.

Essery, R.L.H., Best, M.J., Betts, R.A., Cox, P.M., and Taylor, C.M. 2003. Explicit Representation of Subgrid Heterogeneity in a GCM Land Surface Scheme. *J. Hydrometeor., 4,* 530–543, doi:10.1175/1525-7541(2003)004<0530:EROSHI>2.0.CO;2.

Fairall, C.W., Bradley, E.F., Hare, J.E., Grachev, A.A., and Edson, J.B. 2003. Bulk Parameterization of Air- Sea Fluxes: Updates and Verification for the COARE Algorithm. *J. Clim., 16,* 571–591.

Flocco, D., Schroeder, D., Feltham, D.L., and Hunke, E.C. 2012. Impact of melt ponds on Arctic sea ice simulations from 1990 to 2007. *J. Geophys. Res., 117*, 1–17, doi:10.1029/2012JC008195.

Fox-Kemper, B., Ferrari, R., and Hallberg, R. 2008. Parameterization of mixed layer ddies. Part I: Theory and diagnosis. *J. Phys. Oceanogr., 38,* 1145–1165.

Fox-Kemper, B., Danabasoglu, G., Ferrari, R., Griffies, S.M., Hallberg, R.W., Holland, M.M., Maltrud, M.E., Peacock, S.L., and Samuels, B.L. 2011. Parameterization of mixed layer eddies. III: Implementation and impact in global ocean climate simulations. *Ocean Modelling, 39,* doi:10.1016/j.ocemod.2010.09.002.

Franklin, C.N., Jakob, C., Dix, M., Protat, A., and Roff, G. 2012. Assessing the performance of a prognostic and a diagnostic cloud scheme using single column model simulations of TWP-ICE. *Q. J. R. Meteorol. Soc, 138,* 734–754, doi: 10.1002/qj.954

Franklin, C.N., Sun, Z., Bi, D., Dix, M., Yan, H., and Bodas-Salcedo, A. 2013. Evaluation of clouds in ACCESS using the satellite simulator package COSP. Global, seasonal and regional cloud properties. *J. Geophys. Res., 118,* 732–748. doi: 10.1029/2012JD018469.

Gent, P.R., and McWilliams, J.C. 1990. Isopycnal mixing in ocean circulation models. *J. Phys. Oceanogr., 20,* 150–155.

Gent, P.R. Willebrand, J., McDougall, T.J., and McWilliams, J.C. 1995. Parameterizing eddy-induced tracer transports in ocean circulation models. *J. Phys. Oceanogr., 25,* 463–474.

Gent, P.R., Danabasoglu, G., Donner, L.J., Holland, M.M., Hunke, E.C., Jayne, S.R., Lawrence, D.M., Neale, R.B., Rasch, P.J., Vertenstein, M., Worley, P.H., Yang, Z.L., and Zhang, M. 2011. The Community Climate System Model Version 4. *J. Clim., 24,* 4973–4991.

GLOBE Task Team and others (D.A. Hastings, P.K. Dunbar, G.M. Elphingstone, M. Bootz, H. Murakami, H. Maruyama, H. Masaharu, P. Holland, J. Payne, N.A. Bryant, T.L. Logan, J.-P. Muller, G. Schreier, and J.S. MacDonald), eds., 1999. *The Global Land One-kilometer Base Elevation (GLOBE) Digital Elevation Model, Version 1.0*. National Oceanic and Atmospheric Administration, National Geophysical Data Center, 325 Broadway, Boulder, Colorado 80303, U.S.A. Digital data base on the World Wide Web (URL: http://www.ngdc.noaa.gov/mgg/topo/globe.html) and CD-ROMs.

Gnanadesikan, A., Dixon, K.W., Griffies, S.M., Balaji, V., Barreiro, M., Beesley, J.A., Cooke, W.F., Delworth, T.L., Gerdes, R., Harrison, M.J., Held, I.M., Hurlin, W.J., Lee, H.C., Liang, Z., Nong, G., Pacanowski, R.C., Rosati, A., Russell, J.L., Samuels, B.L., Song, Q., Spelman, M.J., Stouffer, R.J., Sweeney, C., Vecchi, G.A., Winton, M., Wittenberg, A.T., Zeng, F., Zhang, R., and Dunne, J.P. 2006. GFDL's CM2 Global Coupled Climate Models. Part II: The baseline ocean simulation. *J. Clim., 19,* doi:10.1175/JCLI3630.1.

Gordon, H., O'Farrell, S., Collier, M., Dix, M., Rotstayn, L., Kowalczyk, E., Hirst, T., and Watterson, I. 2010. The CSIRO Mk3.5 Climate Model [Electronic resource]. Centre for Australian Weather and Climate Research. GPO Box 1289, Melbourne, Victoria 3001, Australia. *CAWCR Technical Report No. 021*. 61 pp. ISBN: 978-1-921605-666.

Gregory, D. and Rowntree, P.R. 1990. A mass-flux convection scheme with representation of cloud ensemble characteristics and stability dependent closure. *Mon. Weather Rev., 118,* 1483–1506.

Griffies, S.M, 1998. The Gent-McWilliams skew-flux. *J. Phys. Oceanogr., 28,* 831–841.

Griffies, S.M., Gnanadesikan, S. Dixon, K.W., Dunne, J.P., Gerdes, R., Harrison, M.J., Rosati, A., Russell, J., Samuels, B.L., Spelman, M.J., Winton, M., Zhang, R. 2005. Formulation of an ocean model for global climate simulations. *Ocean Science, 1,* 45–79.

Griffies, S.M. 2009. Elements of MOM4p1: GFDL *Ocean Group Tech. Rep. No. 6,* NOAA/Geophysical Fluid Dynamics Laboratory, 444 pp.

Griffies, S.M., Biastoch, A., Boening, C.W., Bryan, F., Chassignet, E., England, M., Gerdes, R., Haak, H., Hallberg, R.W., Hazeleger, W., Jungclaus, J., Large, W.G., Madec, G., Samuels, B.L., Scheinert, M., Gupta, A.S., Severijns, C.A., Simmons, H.L., Treguier, A.M., Winton,

M., Yeager, S., and Yin, J. 2009. Coordinated ocean-ice reference experiments (COREs). *Ocean Modelling, 26,* 1–46, DOI:10.1016/j.ocemod.2008.08.007.

Griffies, S.M., Winton, M., Donner, L.J. Horowitz, L.W., Downes, S.M., Farneti, R., Gnanadesikan, A., Hurlin, W.J., Lee, H.C., Liang, Z. Palter, J.B., Samuels, B.L., Wittenberg, A.T., Wyman, B.L., Yin, J., and Zadeh, N. 2011. The GFDL CM3 Coupled Climate Model: Characteristics of the Ocean and Sea Ice Simulations. *J. Clim., 24,* 3520–3544, DOI: 10.1175/2011JCLI3964.1.

Hewitt, H.T., Copsey, D., Culverwell, I.D., Harris, C.M., Hill, R.S.R., Keen, A.B., McLaren, A.J., and Hunke, E.C. 2011. Design and implementation of the infrastructure of HadGEM3: the next-generation Met Office climate modelling system. *Geosci. Model Dev., 4,* 223–253, doi:10.5194/gmd-4-223-2011.

Hilton, R.D., Featherstone, W.E., Berry, P.A.M., Johnson, C.P.D., and Kirby, J.F. 2003. Comparison of digital elevation models over Australia and external Validation using ERS-1 satellite radar altimetry. *Aust. J. Earth Sci., 50,* 157–168, doi:10.1046/j.1440-0952.2003.00982.x.

Holland, M.M., Bailey, D.A., Briegleb, B.P., Light, B., and Hunke, E. 2012. Improved Sea Ice Shortwave Radiation Physics in CCSM4: The Impact of Melt Ponds and Aerosols on Arctic Sea Ice*. *J. Clim., 25,* 1413–1430. doi: http://dx.doi.org/10.1175/JCLI-D-11-00078.1

Huffman, G.J, Adler, R.F., Bolvin, D.T., and Gu, G. 2009. Improving the Global Precipitation Record: GPCP Version 2.1. *Geophys. Res. Lett., 36,* L17808, doi:10.1029/2009GL040000.

Hunke, E.C., and Dukowicz, J.K. 1997. An Elastic–Viscous–Plastic Model for Sea ice Dynamics. *J. Phys. Oceanogr., 27,* 1849–1867, doi:10.1175/1520-0485(1997)027 <1849:AEVPMF>2.0.CO;2.

Hunke, E.C. and Lipscomb, W.H., 2010. CICE: The Los Alamos sea ice model documentation and software user's manual, Version 4.1. LA-CC-06-012, *Los Alamos National Laboratory*, N.M., 76 pp.

Intergovernmental Panel on Climate Change. 2007. IPCC Fourth Assessment Report, *Climate Change 2007*, UNEP/WMO.

Jochum, M. 2009. Impact of latitudinal variations in vertical diffusivity on climate simulations. *J. Geophys. Res., 114,* C01010, doi:10.1029/2008JC005030.

Jones, P.W. 1997. A User's Guide for SCRIP: A spherical coordinate remapping and interpolation package. LA-CC- 98-45, *Los Alamos National Laboratory*, N.M., 27pp.

Kim, D., Kug, J.-S., Kang, I.-S., Jin F.-F., and Wittenberg, A.T. 2008. Tropical Pacific impacts of convective momentum transport in the SNU coupled GCM. *Clim. Dyn., 31,* 213–226. DOI 10.1007/s00382-007-0348-4.

King, J.C., Connolley, W.M. and Derbyshire, S.H. 2001. Sensitivity of modelled Antarctic climate to surface and boundary-layer parametrizations. *Q. J. R. Meteorol. Soc., 127*, 779–794.

Kowalczyk, E.A., Wang, Y.P., Law, R.M., Davies, H.L., McGregor, J.L., and Abramowitz, G. 2006. The CSIRO Atmosphere Biosphere Land Exchange (CABLE) model for use in climate models and as an offline model. *CSIRO Marine and Atmospheric Research paper 013,* 43pp. www.cmar.csiro.au/e-print/open/kowalczykea_2006a.pdf

Kowalczyk, E.A., Stevens, L., Law, R.M., Dix, M., Wang, Y.P., Harman, I.N., Hayens, K., Srbinovsky, J., Pak, B., and Zhien, T. 2013. The land surface model component of ACCESS: description and impact on the simulated surface climatology. *Aust. Met. Oceanogr. J.*, 63, 65–82..

Kwok, R., and Cunningham, G.F. 2008. ICESat over Arctic sea-ice: Estimation of snow depth and ice thickness. *J. Geophys. Res., 113,* C08010, doi:10.1029/2008JC004753.

Large, W.G., McWilliams, J.C., and Doney, S.C. 1994. Oceanic vertical mixing: A review and a model with a nonlocal boundary layer parameterization. *Rev. Geophys., 32*, 363–403, doi:10.1029/94RG01872.

Laxon, S., Peacock, N. and Smith, D. 2003. High interannual variability of sea ice thickness in the Arctic region. *Nature, 425*, 947–950.

Lock, A.P, Brown, A.R., Bush, M.R., Martin G.M. and Smith, R.N.B. 2000. A new boundary layer mixing scheme. Part I: Scheme description and single-column model tests. *Mon. Weather Rev., 128,* 3187–3199

Leuning, R. 1995. A critical appraisal of a combined stomatal photosynthesis model for C3 plants. *Plant Cell Environ., 18,* 339–355, doi:10.1111/j.1365-3040.1995.tb00370.x.

Lin, J. L. 2007. The double-ITCZ problem in IPCC AR4 coupled GCMs: ocean-atmosphere feedback analysis. *J. Clim., 20,* 4497–4525.

Locarnini, R., Mishonov, A., Antonov, J., Boyer, T., Garcia, H. 2006. *World Ocean Atlas 2005*, volume 1: Temperature. U.S. Government Printing Office 61, NOAA Atlas NESDIS, Washington, DC, 182 pp.

Lock, A.P., Brown, A.R, Bush, M.R., Martin, G.M., and Smith, R.N.B. 2000. A new boundary layer mixing scheme. Part I: Scheme description and SCM tests. *Mon. Weather Rev., 128,* 3187–3199.

Lucarini, V., and Ragone, F. 2011. Energetics of PCMDI/CMIP3 climate models: energy budget and meridional enthalpy transport. *Rev Geophys., 49,* RG1001. DOI:10.1029/2009RG000323.

McDougall, T. J., 2003: Potential enthalpy: a conservative oceanic variable for evaluating heat content and heat fluxes. *J. Phys. Oceanogr., 33,* 945–963.

Marsland, S.J., Bi, D., Uotila, P., Fiedler, R., Griffies, S.M., Lorbacher, K., O'Farrell, S., Sullivan, A., Uhe, P., Zhou, X., and Hirst, A.C. 2013. Evaluation of ACCESS Climate Model ocean diagnostics in CMIP5 simulations. *Aust. Met. Oceanogr. J.*, 63, 101–119.

Martin, G.M., Milton, S.F., Senior, C.A., Brooks, M.E., Ineson, S., Reichler, T., and Kim, J. 2010. Analysis and Reduction of Systematic Errors through a Seamless Approach to Modelling Weather and Climate. *J. Clim., 23,* 5933–5957, doi:10.1175/2010JCLI3541.1.

Martin, G.M., Ringer, M.A., Pope, V.D., Jones, A., Dearden, C., and Hinton, T.J. 2006. The physical properties of the atmosphere in the new Hadley Centre Global Environment Model, HadGEM1. Part I: Model description and global climatology. *J. Clim., 19,* 1274–1301.

Martin, G.M., Bellouin, N., Collins, W.J., Culverwell, I.D., Halloran, P., Hardiman, S., Hinton, T.J., Jones, C.D., McLaren, A., O'Connor, F., Rodriguez, J., Woodward, S., et al. 2011. The HadGEM2 family of Met Office Unified Model climate configurations. *Geosci. Model Dev. Discuss., 4,* 723–757, doi:10.5194/gmd-4-723-2011.

Meehl, G.A., Stocker, T.F., Collins, W.D., Friedlingstein, P., Gaye, A.T., Gregory, J.M., Kitoh, A., Knutti, R., Murphy, J.M., Noda, A., Raper, S.C.B., Watterson, I.G., Weaver A.J., and Zhao. Z.-C. 2007. Global Climate Projections. In: *Climate Change 2007: The Physical Science Basis. Contribution of Working Group I to the Fourth Assessment Report of the Intergovernmental Panel on Climate Change* [Solomon, S., D. Qin, M. Manning, Z. Chen, M. Marquis, K.B. Averyt, M. Tignor and H.L. Miller (eds.)]. Cambridge University Press, Cambridge, United Kingdom and New York, NY, USA.

Murray, R.J. 1996. Explicit generation of orthogonal grids for ocean models. *J. Comput. Phys., 126,* 251–273.

Pacanowski, R.C. and Gnanadesikan, A. 1998. Transient response in a z-level ocean model that resolves topography with partial-cells. *Mon. Weather Rev., 126,* 3248–3270.

Pincus R., Batstone, C.P., Patrick-Hofmann, R.J., Taylor, K.E., and Gleckler, P.E. 2008. Evaluating the present-day simulation of clouds, precipitation and radiation in climate models. *J. Geophys. Res., 113,* D14209, doi:10.1029/2007JD009334.

Pirazzini, R. 2008. Factors controlling the surface energy budget over snow and ice. *Finnish Meteorolog. Inst. Contributions, 75,* 1–55.

Puri, K., G. Dietachmayer, P. Steinle, M. Dix, L. Rikus, L. Logan, M. Naughton, C. Tingwell, Y Xiao, V. Barras, I. Bermous, R. Bowen, L. Deschamps, C. Franklin, J. Fraser, T. Glowacki, B. Harris, J. Lee, T. Le, G. Roff, A. Sulaiman, H. Sims, X. Sun, Z. Sun, H. Zhu, M. Chattopadhyay, C. Engel. 2013. Implementation of the initial ACCESS Numerical Weather Prediction system. *Aust. Met. Oceanogr. J.*, in press.

Rashid, H.A., Hirst, A.C. and Dix, M. 2013a. Atmospheric circulation features in the ACCESS coupled model simulations for CMIP5: Historical simulation and future projections. *Aust. Met. Oceanogr. J.*, 63, 145–160.

Rashid, H.A., Sullivan, A., Hirst, A.C., Bi, D., and Marsland, S.J. 2013b. Evaluation of El Nino-Southern Oscillation in the ACCESS coupled model simulations for CMIP5. *Aust. Met. Oceanogr. J.*, 63, 161–180.

Rahmstorf, S. 1993. A fast and complete convection scheme for ocean models. *Ocean Modelling, 101,* 9–11.

Rayner, N.A., Parker, D.E., Horton, E.B., Folland, C.K., Alexander, L.V., Rowell, D.P., Kent, E.C. and Kaplan, A. 2003. Global analyses of sea surface temperature, sea ice, and night marine air temperature since the late nineteenth century. *J. Geophys. Res., 108,* No. D14, 4407, doi:10.1029/2002JD002670.

Rossow, W.B. and Sciffer, R.A. 1999. Advances in understanding clouds from ISCCP. *Bull. Am. Meteorol. Soc., 80,* 2261–2287

Rossow, W.B. and Garner, L.C. 1993. Validation of ISCCP Cloud Dections. *J. Clim., 6,* 2370–2393.

Rotstayn, L.D., Jeffrey, S.J., Collier, M.A., Dravitzki, S.M., Hirst, A.C., Syktus, J.I., and Wong, K.K. 2012. Aerosol and greenhouse gas-induced changes in summer rainfall and circulation in the Australasian region: a study using single-forcing climate simulations. *Atmos. Chem. Phys., 12,* 6377–6404, doi:10.5194/acp-12-6377-2012.

Scaife, A.A., Butchart, N., Warner, C.D. and Swinbank, R. 2002. Impact of a spectral gravity wave parameterization on the stratosphere in the Met. Office Unified Model. *Q. J. R. Meteorol. Soc., 59,* 1473–1489.

Semtner, A.J. 1976. A model for the thermodynamic growth of sea ice in numerical investigations of climate. *J. Phys. Oceanogr., 6,* 379–389.

Sen Gupta, A., Muir, L.C., Brown, J.N., Phipps, S.J., Durack, P.J., Monselesen, D., and Wijffels, S.E. 2012. Climate drift in CMIP3 models. *J. Clim., 25,* 4621–4640.

Shonk, J.K.P. and Hogan, R.J. 2008. Tripleclouds: an efficient method for representing cloud inhomogeneity in 1D radiation schemes by using three regions at each height. *J. Clim., 21,* 2352–2370.

Smith, R.N.B. 1990. A scheme for predicting layer clouds and their water contents in a general circulation model. *Q. J. R. Meteorol. Soc., 116,* 435–460.

Smith, I. 2007. Global climate modelling within CSIRO: 1981 to 2006. *Aust. Meteorol. Mag., 56,* 153–166.

Stephens, G.L., Tsay, S.C., Stackhouse Jr, P.W., and Flatau, P. 1990. The relevance of the microphysical and radiative properties of cirrus clouds to climate and climate feedback. *J. Atmos. Sci., 47,* 1742–1753.

Stouffer, R.J. 2004. Time Scales of Climate Responses. *J. Clim., 17,* 209–217.

Sun, Z.C. Franklin, X. Zhou, Y. Ma, P. Okely, D. Bi, M. Dix, A.C. Hirst, J. K.P. Shonk, and K. Puri, 2013. Modifications in atmospheric physical parameterization for improving SST simulation in the ACCESS coupled model. *Aust. Met. Oceanogr. J., 63,* 233–247.

Taylor, K.E., Stouffer, R.J. and Meehl, G.A., 2009. A summary of the CMIP5 experiment design. PCDMI Rep., 33 pp. [http://cmip-pcmdi.llnl.gov/cmip5/docs/Taylor_CMIP5_design.pdf]

Taylor, K.E., Stouffer, R.J., Meehl, G.A. 2012. An Overview of CMIP5 and the experiment design. Bull. *Amer. Meteor. Soc., 93,* 485–498, doi:10.1175/BAMS-D-11-00094.1.

Trenberth, K.E., and Fasullo, J.T. 2010. Simulation of present day and 21st century energy budgets of the southern oceans. *J. Clim., 23,* 440–454, doi:10.1175/2009JCLI3152.1.

Uotila, P., O'Farrell, S., Marsland, S.J., and Bi, D. 2012. A sea ice sensitivity study with a global ocean-ice model. *Ocean Modelling, 18,* doi:http://dx.doi.org/10.1016/j.ocemod.2012.04.002.

Uotila, P., O'Farrell, S., Marsland, S.J., and Bi, D. 2013. The sea ice performance of the Australian models participating in the CMIP5. *Aust. Met. Oceanogr. J.,* 63, 121–143.

Valcke, S. 2006. OASIS3 User Guide (prism 2-5). PRISM Support Initiative No 3, 68 pp.

Voldoire, A., Sanchez-Gomez, E., Salas y Me´lia, D., Decharme, B., Cassou, C., Se´ne´si, S., Valcke, S., Beau, I., Alias, A., Chevallier, M., De´que´, M., Deshayes, J., Douville, H., Fernandez, E., Madec, G., Maisonnave, E., Moine, M.P., Planton, S., Saint-Martin, D., Szopa, S., Tyteca, S., Alkama, R., Belamari, S., Braun, A., Coquart, L., and Chauvin, F. 2012. The CNRM-CM5.1 global climate model: description and basic evaluation. *Clim. Dyn.,* DOI 10.1007/s00382-011-1259-y.

Wang, Y.P. and Leuning, R. 1998. A two-leaf model for canopy conductance, photosynthesis and partitioning of available energy I. Model description and comparison with a multi-layered model. *Agric. Forest Meteor., 91,* 89–111.

Wang, Y.P., Kowalczyk, E.A., Leuning, R., Abramowitz, G., Raupach, M.R., Pak, B., van Gorsel, E. and Luhar, A. 2011. Diagnosing errors in a land surface model (CABLE) in the time and frequency domains. *J. Geophys. Research-Biogeosciences, 116.* G01034, doi:10.1029/2010JG001385.

Warner, C.D. and McIntyre, M.E. 2001. An Ultrasimple Spectral Parameterization for Nonorographic Gravity Waves. *J. Atmos. Sci., 58,* 1837–1857.

Watterson, I.G. 1996. Non-dimensional measures of climate model performance. *Int. J. Climatol., 16,* 379–391.

Watterson, I.W., Hirst, A.C. and Rotstayn, L.D. 2013. A skill-score based evaluation of simulated Australian climate. *Aust. Met. Oceanogr. J.,* 63, 181–190.

Webster, S., Brown, A.R., Cameron, D.R. and Jones, C.P. 2003. Improvements to the representation of orography in the Met. Office Unified Model. *Q. J. R. Meteorol. Soc., 129,* 1989–2010.

Williams, D.N., Ananthakrishnan, R., Bernholdt, D.E., Bharathi, S., Brown, D., Chen, M., Chervenak, A.L., Cinquini, L., Drach, R., Foster, I.T., Fox, P., Fraser, D., Garcia, J., Hankin, S., Jones, P., Middleton, D.E., Schwidder, J., Schweitzer, R., Schuler, R., Shoshani, A., Siebenlist, F., Sim, A., Strand, W.G., Su, M., and Wilhelmi, N. 2009. The Earth System Grid - Enabling Access to Multimodel Climate Simulation Data.Bul. *Am. Met. Soc., 90,* 195–205.

Williams, K.D., Ringer, M.A., Senior, C.A., Webb, M.J., McAvaney, B.J., Andronova, N., Bony, S., Dufresne, J.L., Emori, S., and Gudgel, R. 2006. Evaluation of a component of the cloud response to climate change in an intercomparison of climate models. *Clim. Dyn., 26,* 145–165.

Wilson, D.R., Smith, R.N.B., Gregory, D., Wilson, C., Bushell, A.C. and Cusack, S. 2004. The Large-Scale Cloud Scheme and Saturated Specific Humidity. *Unified Model Documentation Paper 26.* Available from Met Office.

Wilson, D.R. and Ballard, S.P. 1999. A microphysically based precipitation scheme for the UK Meteorological Office Unified Model. *Q. J. R. Meteorol. Soc, 125,* 1607–1636

Wilson, D.R., Bushell, A.C., Kerr-Munslow, A.M., Price, J.D., and Morcrette, C.J. 2008. PC2: A prognostic cloud fraction and condensation scheme. I: Scheme description, *Q. J. R. Meteorol. Soc., 134,* 2093–2107.

Wood, N., Diamantakis, M., Staniforth, A. 2007. A monotonically damping, second-order accurate, unconditionally stable, numerical scheme for diffusion An improved implicit predictor-corrector scheme for boundary layer vertical diffusion. *Q. J. R. Meteorol. Soc. 133,* 1559–1573.

Worby, A., Geiger, C.A., Paget, M.J., Van Woert, M.L., Ackley, S.F., and DeLiberty, T.L. 2008. Thickness distribution of Antarctic sea-ice. *J. Geophys. Res., 617,* 1-14, doi:10.1029/2007JC004254.

Wu, X.Q., Deng, L., Song, X., Zhang, G.J. 2007. Coupling of convective momentum transport with convective heating in global climate simulations. *J. Atmos. Sci., 64,* 1334–1349.

Yao, M.S., and Del Genio, A.D. 1999. Effects of cloud parameterization on the simulation of climate changes in the GISS GCM. *J. Clim., 12,* 761–779.

Yao, M.S. and Del Genio, A.D. 1999. Effects of cloud parameterization on the simulation of climate changes in the GISS GCM. *J. Clim., 12,* 761–779.

Zheng, X.T., Xie, S.P., Vecchi, G.A., Liu, Q. and Hafner, J. 2010. Indian Ocean dipoleresponse to global warming: Analysis of ocean-atmospheric feedbacks in a coupled model. *J. Clim., 23,* 1240–1253.